Model Development and Numerical Simulation of Thermo-Sensitive Hydrogel and Microgel-Based Drug Delivery

WANG ZIJIE

(B.Eng. & M.Eng., Wuhan University of Technology, P. R. China)

A THESIS SUBMITTED

FOR THE DEGREE OF MASTER OF ENGINEERING

DEPARTMENT OF MECHANICAL ENGINEERING

NATIONAL UNIVERSITY OF SINGAPORE

2004

Acknowledgement

This thesis has become possible due to the generous and ongoing support of many people. I would like to take this opportunity to express my deepest and sincere appreciation to them.

First and foremost, I would like to thank my supervisor, Prof. Lam Khin Yong for his dedicated support, guidance, and critical comments throughout the course of research and study. Prof. Lam's invaluable advice will benefit me a lot in my following life.

I am deeply indebted to my co-supervisor Dr. Li Hua, whose help, stimulating suggestions and encouragement helped me in all the time of the present research and writing of this thesis. Dr. Li Hua's influence on me is far beyond this thesis, and his dedication to research and preciseness inspire me in my future work.

Specially, I want to thank Dr. Wang Xiaogui for his contribution and support throughout the course of study and programming on the research of thermo-sensitive hydrogels. Also, I would like to thank Drs. Wu Shunnian and Yan Guoping for their contributions and advices on the research of microgel-based drug delivery system.

Besides, I wish to give thanks to my colleagues and friends Mr. Yew Yong Kin, Chen Jun, Luo Rongmo and Zhang Jian for their encouragement, help and friendship during the course of research and study.

Finally, I greatly appreciate the constant support, love and concerns of my parents and sister.

Table of Contents

Summary

Recently the bio-stimulus responsive hydrogels have been attracting much attention because of their scientific interest and technological importance. In this dissertation, two mathematical models are presented for simulation of the hydrogels. One is a steady-state model for responsive behaviors of thermo-sensitive hydrogels, and the other is a transient model for drug release from microgels. These developed models, consisting of linear/nonlinear partial differential equations coupled with a transcendental equation, are solved by the novel true meshless Hermite-cloud method.

For simulation of swelling equilibrium of temperature-stimulus-responsive hydrogels, a novel multiphysical steady-state model, termed the Multi-Effect-Coupling thermal-stimulus (MECtherm) model, has been developed to simulate and predict the volume phase transition of the neutral and ionized thermo-sensitive hydrogels when they are immersed in bathing solution. The developed MECtherm model is based on the Flory's mean field theory and includes the steady-state Nernst-Planck equations simulating the distributions of diffusive ionic species, the Poisson equation simulating the electric potential, and a transcendental equation for swelling equilibrium. The MECtherm model is validated by comparing the numerical results with the experimental data published in open literature. Variations of volume phase transition with temperature are simulated and discussed under different initial fixed charge densities, bathing solution concentrations, effective crosslink densities and initial polymer volume fractions, respectively. The distributions of several key physical parameters in both internal hydrogels and external bathing solution before and after the volume phase transition are compared and investigated, which include

the mobile cation and anion concentrations, fixed charge density and electrical potential.

For study of microgel-based drug delivery system, a transient mathematical model is presented to simulate the controlled nifedipine release from chitosan spherical micro gels, in which both the drug dissolution and diffusion are taken into account through the continuous matrices of spherical microgels. Using this model, the drug diffusion coefficient and drug dissolution rate constant are identified numerically. The effects of several important physical parameters on drug release are simulated and discussed in details, which include the microgel radius, drug saturation concentration, drug diffusion coefficient and drug dissolution rate constant. The present studies and discussions are useful for practical designers to analyze and optimize the controlled drug release process.

Nomenclature

A	area of microgels
b	empirical parameter
C	concentration of solute dissolved in microgels
C_0	initial solute loading in microgels
C_s	drug saturation concentration in microgels
$\overline{C}$	non-dimensional concentration of solute dissolved in microgels
c_f	fixed-charge density
c_j	the *j*th mobile ion concentration in the interior hydrogels
c_j^*	the *j*th mobile ion concentration in the exterior bathing solution
c_{ref}	reference parameter
$\overline{c_j}$	non-dimensional concentration of the *j*th ion
$\overline{c_f}$	non-dimensional fixed charge concentration
d	total drug content
D	drug diffusion coefficient
D_j	diffusion coefficient of the *j*th ion
F	Faraday constant
J	drug diffuse flux

ΔG_{gel}	total free energy change within the hydrogels
ΔG_{Mixing}	free energy change by the mixing contribution
$\Delta G_{Elastic}$	free energy change by the elastic deformation contribution
ΔG_{Ion}	free energy change by the ionic contribution
k	dissolution rate constant
k_B	Boltzmann constant
m	mass of drug-loaded microgels
L_{ref}	reference parameter
M_t	absolute cumulative amount of drug released at time t
M_∞	absolute cumulative amount of drug released at time t=∞
R	mean radius of dry microgels, cm
R_0	radius of cylindrical hydrogel at the reference state
s_{12}	degeneracy ratio
r	radial position in hydrogels
T	absolute temperature
t	release time
$\boldsymbol{u}$	displacement vector
z	lattice coordination number
z_f	valence of fixed charge

z_j	valence of *j*th mobile ion
α	linear volume swelling ratio
β	non-dimensional dissolution/diffusion number
δh	change of enthalpy per monomeric unit of the network
δs	change of entropy per monomeric unit of the network
εC_s	equivalent drug saturation concentration
ζ	interchange energy
ζ_{12}	difference of the segmental interaction energy
λ	a weighted coefficient ($0 \le \lambda \le 1$)
$\Delta\mu_{gel}$	change of chemical potential of the solvent within the hydrogel
$\Delta\mu^*_{Ion}$	change of chemical potential of the solvent in the external solution.
ξ	non-dimensional radius
τ	non-dimensional Fourier time
υ	molar volume of the solvent
ϕ	polymer-network volume fraction at swelling equilibrium state
ϕ_0	initial polymer-network volume fraction in the pregel solution
χ	polymer-solvent interaction parameter
χ_2	experiment-based adjustable parameter
v_e	effective crosslink density

ψ	electric potential.
$\overline{\psi}$	non-dimensional electrical potential
ψ_{ref}	reference parameter

List of Figures

List of Tables

Chapter 1

Introduction

This chapter provides the background of the present studies. The formation and characteristics of the hydrogels are briefly described first. They are followed by a literature survey on the research history and application of the hydrogel, especially focusing on the temperature sensitive hydrogels and microgel-based drug delivery systems. Then the objectives and scopes of the present work are presented, and lastly the layout of the dissertation is given.

1.1 Definition of environment stimuli responsive hydrogels

Hydrogels are three-dimensional crosslinked macromolecular networks that typically embody three phases, namely solid matrix network, interstitial fluid and ionic species. Individual molecules called monomers, such as amino acids, can be chemically chained together to make polymers. Replacing some of these monomers by the crosslinks, which can make multiple bonds or strong physical forces, allows these polymers to connect each other to form a network, as illustrated in Figure 1.1.

Hydrogels are interesting materials with both solid-like and liquid-like properties. The solid-like properties result from crosslinked polymeric network, which make the hydrogels have a shear modulus. As such, the hydrogels can retain geometric shape when they are deformed. The liquid-like properties are owing to the fact that the hydrogel networks can absorb enough solution, in which the major constituent of hydrogels is usually liquid. In the mechanical properties, the hydrogels have high deformability and nearly complete recoverability, which are the most

important property of swelling degree or swelling ratio for the hydrogels. For example, some hydrogels can reversibly swell and shrink by as much as several times of their original size in response to small changes in environmental conditions (Onuki, 1993). The polymer chains can either attract each other and be very compact, or repel each other and be swollen, depending on different environmental conditions. Figure 1.2 shows schematically the two states of hydrogels (Shibayama, 1993), namely the collapsed and swollen states, which correspond to the liquid and the gas states of fluids, respectively. These changes may occur discontinuously at a specific stimulus level, which is called a volume phase transition, or gradually over a range of stimulus values (Wang et al. 1993). The specific environmental stimuli that make polymeric hydrogels change their solvent-swollen volumes include the temperature (Roberto et al., 1987), solution pH (Gehrke, 1989), externally applied electric field (Grimshaw, 1990), solvent quality (Ohmine et al., 1982), light intensity and wavelength (Mamada et al., 1990), pressure (Kato, 2000), ionic strength (Hirotsu et al., 1987), ion identity (Annaka et al., 2000) and specific chemical triggers like glucose (Gehrke, 1993). For example, the temperature-sensitive hydrogels perform the sudden volume changes with small changes in temperature. From this perspective, these hydrogels are also termed as “actuated”, “stimuli sensitive”, and “smart” materials.

As described by Shibayama (1993), extensive progress has been made in the technological applications of hydrogels. For example, disposable diapers and sanitary napkins use hydrogels as super water-absorbents. Hydrogel sheets are developed to keep fish and meat fresh. Hydrogels are indispensable materials as a molecular sieve for molecular separation, such as hydrogel permeation chromatography and electrophosphoresis. Temperature and/or pH sensitive hydrogels are developed as drug delivery systems in the human body, where the hydrogel releases drug gradually

or suddenly at a particular location in the body in response to the changes of temperature and/or pH around the hydrogel. As illustrated previously, an enormous change in hydrogel volume can be induced by a small change of the stimuli and this is of great importance in its application, such as actuator, sensor, switching device and so on (Tanaka, 1981).

1.2 Literature survey

Katchalsky (1949) is the first who created the responsive polymeric hydrogels by crosslinking water-soluble poly-electrolytes to form hydrogels which can swell and shrink in response to changes in solution pH. Later studies include the work of Dusek et al. (1968), postulating that the swollen and shrunken phases of hydrogel could coexist and the transition between the two states would occur at a fixed value of surrounding environment. Tanaka (1978) observed such a phase transition in the ionized poly-acrylamide hydrogels at specific concentrations of acetone in water. Tanaka's research group and others also demonstrated that the discontinuous phase transition should be observable in all hydrogel/solvent systems. Since mid-1980s, study of responsive polymeric hydrogels has attracted the attention of numerous researchers worldwide.

Due to the scientific and technological importance of the hydrogels, extensive research efforts have been made recently. In this dissertation however, only two kinds of the hydrogels are investigated. One is thermo-sensitive hydrogels, in which the temperature stimulus is the main source for their volume phase transition. The other is microspheric hydrogels that are called microgels and are used as drug delivery

carriers, in which the drug concentration is the main driving force for the drug delivery process.

1.2.1 Temperature-stimulus-responsive hydrogels

In the various responsive hydrogels to environment stimuli, the temperature-stimulus-responsive hydrogels have been extensively studied since they have wide-range applications such as in drug delivery systems (Onuki, 1993), sensor and actuators (Li and Tanaka, 1992). For the temperature-sensitive hydrogels, the volume phase transitions are generally classified into three categories, thermo-swelling, thermo-shrinking, and convexo (Otake et al., 1990). The thermo-swelling hydrogel expands with increasing temperature (Tanaka, 1978), the thermo-shrinking one contracts with temperature (Hirokawa, 1984) and the convexo one expands or contracts depending upon conditions (Katayama et al., 1984). According to the work of Otake et al. (1990), the types of volume phase transition are greatly affected by the affinity between solvent and monomer units within the hydrogel. For example, thermo-swelling hydrogels contain mostly hydrophilic monomers. Thermo-shrinking hydrogels are composed of monomers that contain hydrophobic substituents. The phenomenon of volume phase collapse transitions were firstly observed by Tanaka (1978). For convenience of studying the transition characteristics, a Lower Critical Solution Temperature (LCST) is defined for the temperature of the surrounding solution of the hydrogels. When the solution temperature is below LCST, the hydrogels perform in a hydrophilic and soluble state. If the temperature is above LCST, the polymer chains become hydrophobic, and the hydrogels collapse, expel water and shrink in volume. For example, aqueous crosslinked poly(*N*-

isopropylacrylamide) (PNIPA) hydrogels exhibit its own LCST at approximate 33°C (Beltran et al., 1990).

Many potential applications of the temperature-stimulus-responsive hydrogels require the incorporation of fixed charges attached on the polymeric chains of the hydrogel network, which are also called the ionic hydrogels. Ionic groups may be used for imparting to a specific solute binding or exclusion properties, or for increasing the water absorption capacity of the hydrogel. Obviously, the fixed charges in hydrogels have significant influence on the temperature induced phase transitions. Hirotsu et al. (1987) and Beltran et al. (1990) further showed that the temperature-dependent swelling equilibrium of the hydrogel in water or in electrolyte is highly dependent on the degree of hydrogel ionization.

Since Katchalsky (1949) first found the responsive polymeric hydrogels, many researchers have made their efforts on the theoretical study of the swelling equilibrium of hydrogels. In 1953, Flory proposed a thermodynamic framework for interpreting the swelling equilibrium of hydrogel and solution properties. However, the framework is often unsuitable for hydrogels, which are characterized by orientation-dependent strong interactions. A lattice fluid theory with consideration of the holes in the lattice as a component was developed by Sanchez and Lacombe (1976) to describe the effects of volume changes on polymers, polymer solutions and mixtures, but it has been criticized since it does not afford a satisfactory description of polymer melts over a wide range of pressures (Zoller, 1980). Tanaka et al. (1978, 1980) also attempted to explore the theoretical studies on volume phase transitions by the Flory-Huggins theory (Flory, 1953), which is a mean field theory to qualitatively describe the phase transition (Li and Tanaka, 1992).

In the study of the temperature-stimulus-responsive hydrogels, the first recorded work was done by Ilavsky (1982). Later works include several phase-transition investigations based on different theories, instead of the Flory-Huggins theory. Otake et al. (1989) proposed a theoretical model with the hydrophobic interaction for explaining the thermally induced discontinuous volume collapse of hydrogels. Prange et al. (1989) incorporated the influence of hydrogen bonding and described the phase behavior of these systems, in which three energy parameters were obtained from liquid-liquid equilibrium (LLE) for a swelling equilibrium linear PNIPA/water system using an oriented quasi-chemical model. The resulting model is able to present the major features of LCST behavior in aqueous solutions of linear polymer and polymer hydrogels. Painter et al. (1990) also attempted to consider the effects of hydrogen bonding on the hydrogel thermodynamic properties. The extent of the hydrogen bonding is quantified by an equilibrium constant, which must be determined from experimental data. Beltran et al. (1990) and Hooper et al. (1990) investigated the swelling behaviors of hydrogels prepared by copolymerizing PNIPA with strong electrolyte, and predicted the swelling behaviors of positively ionized hydrogels in sodium chloride solution using the quasi-chemical model combining the ideal Donnan theory (Flory, 1953) with Flory and Erman's (1986) elastic model. Hooper et al. (1990) studied the effects of total monomer concentration and crosslink density on swelling capacity. Marchetti et al. (1990) introduced Sanchez and Lacombe's lattice-fluid model that considered voids to be a component in lattice for the free energy of mixing.

Recently, many scientists continuously make their efforts on the volume phase transition of temperature-sensitive hydrogels. In the model proposed by Sasaki and Maeda (1996), the influence of polymer-water interactions on the hydrogel phase

transition was included through a function of experimentally determined chemical potential for water molecules. Lele et al. (1995, 1997) used an extended version of Sanchez and Lacombe's (1978) theory with the hydrogen-bonding effects. Different from the approach of Prausnitz and co-workers (1989), a temperature-dependent interaction parameter is used to describe the volume transition of PNIPA hydrogels with increasing temperature. Hino and Prausnitz (1998) presented a model that extends Flory-Huggins theory by considering Flory's interaction parameter as a product of temperature and composition dependent term, in which the temperature-dependent contribution includes the effects of specific interactions such as hydrogen bonding. One of the advantages of this model is its similarity with the classical Flory-Rehner theory (Flory, 1953) for hydrogels but the specific oriented interactions are bundled into a pair of interaction dependent parameters.

Although many theoretical models were developed, it is still difficult to predict well the phenomena of volume phase transition, when compared with experimental swelling data, especially in high degree of swelling. Furthermore, most theoretical models are unable to analyse the swelling behaviors of ionized hydrogels. In order to overcome the difficulty, a novel multiphasic model has been developed in this dissertation for simulation of the swelling equilibrium of temperature-sensitive hydrogels with fixed charges.

1.2.2 Microgel-based drug delivery system

In development of bioengineering and biotechnology, one of studies attracting the attention of most researchers is microgel-based controlled drug delivery system, as reviewed by Tanaka (1981), Hoffman (1987), Li and Tanaka (1992) and Gehrke (1993). The controlled drug delivery systems investigated include various polymer-

based microgels, such as spherical chitosan microgels (Chandy and Sharma, 1992; Filipovic et al., 1996), Eudragit microgels (Hombreiro et al. 2003) and poly(DL-lactide-co-glycolide acid) microgels (Soppimath and Aminabhavi, 2002; Dhawan 2003). Compared with conventional methods, the microgel-based drug delivery system can reduce the total administration frequency to the patient. It can also be cycled over a long period, or triggered by specific environment or external events. Microgel-based drug release maintains the drug at desired levels over a long period and thus eliminates the potential for both under- and overdosing. Consequently, it decreases the possible adverse effects of immediate drug release. Additional advantages of microgel-based drug delivery include optimal dosage administration, better patient compliance and improved drug efficacy. In general, when drug-loaded polymeric microgels are placed in contact with release medium, the drug release process is divided into four consecutive steps (Hombreiro et al., 2003): (1) the imbibition of release medium into the microspherical system driven by osmotic pressure arising from concentration gradients; (2) drug dissolution; (3) drug diffusion through the continuous matrices of microgels due to concentration gradients; and (4) drug diffusional and convective transport within the release medium. One or more of these steps can control the drug release process.

Currently the theoretical understanding of underlying drug release mechanisms by polymer-based microgels is still at beginning stage, since most works are experimental-based. Few efforts have been made on the theoretical understanding and model development. For example, Varshosaz and Falamarzian (2001) claimed that drug release process could be via the diffusion through the continuous matrices or drug dissolution mechanism. In the diffusion mechanism, drug diffusion through the continuous matrices of microgels controls the drug release process, whereas in the

dissolution mechanism the drug release is controlled by the process involving drug dissolution within the microgels followed by drug diffusion through the continuous matrices of microgels. However, the drug release process is usually modeled with the classical Fick's diffusion equation integrating with appropriate boundary conditions or with the simplified expressions developed by Higuchi T. (1961) and Higuchi W. (1962, 1970). A mathematical theory with simultaneous consideration of drug dissolution and diffusion in the continuous matrices of microgels was put forward by Grassi et al. (2000) and well fitted to the experimentally measured temazeoan and medroxyprogesterone acetate release data. Recently, Hombreiro-Perez et al. (2003) pointed out that an adequate description of nifedipine release from microgels must consider drug dissolution, drug diffusion in the continuous matrices of microgels and the limited solubility of nifedipine in the release medium. Unfortunately, no effort is made to model the nifedipine release process due to the complexity.

1.3 Objectives and scopes

As mentioned above, majority of previously published studies on the hydrogels are experimentally-based, and few theoretical efforts have been made. Sometimes in experimental analysis it is not convenient to measure the hydrogels with more complex shapes and the accurate dimensional change of their volume transition behaviors. The prediction of hydrogel performance by modeling and simulation will thus be critical for understanding the characteristics of hydrogels. In a situation where hydrogel characteristics have to be optimized for a particular application, a ready modeling and simulation will prove indispensable.

The aims of this dissertation are composed of two parts. The first is to develop a steady-state mathematical model for simulation of the volume phase transition of neutral/ionic thermo-sensitive hydrogels immersed in water or electrolyte solution, respectively. The second is to enhance a transient mathematic model for simulation of the drug delivery from the microgels. Both the mathematic models, consisting of nonlinear/linear partial differential equations, are solved numerically by the novel true meshless Hermite-Cloud method provided by Li et al. (2003).

In the steady-state analysis of volume phase transition of thermo-sensitive hydrogels, poly(*N*-isopropylacrylamide) (PNIPA) hydrogel is chosen and studied here since it is a typical example of the hydrogels which show a thermo-shrinking phase transition in aqueous or electrolyte solutions, where an increasing temperature causes the hydrogel to shrink geometrically by one order of magnitude. The neutral hydrogel is a relatively simple system, and can undergo a volume phase transition in pure water in response to temperature change. In the present study, a coupled chemo-electro-thermo-mechanical multiphysical model, termed the Multi-Effect-Coupling thermal-stimulus (MECtherm) model, is developed mathematically to simulate and predict the volume phase transition of the neutral and ionized thermo-sensitive hydrogels when they are immersed in bathing solution. The developed MECtherm model is based on the Flory's mean field theory, and includes the steady-state Nernst-Planck equations simulating the distribution of diffusive ionic species, the Poisson equation simulating the electric potential and a transcendental equation for swelling equilibrium. In evaluating the mathematic model, Hirotsu's (1987) experimental data are used for comparison with the numerical simulation results. Variations of volume phase transition with temperature are simulated and discussed under different initial fixed charge densities, bathing solution concentrations, effective crosslink densities and

initial polymer volume fractions, respectively. The distributions of several important physical parameters in both internal hydrogels and external bathing solution before and after the volume phase transition are compared and investigated, which include the mobile cation and anion concentration, fixed charge density and electrical potential.

In the transient analysis of microgel-based drug delivery system, the nifedipine release from the spherical chitosan microgels is investigated numerically with a relatively simple mathematical model in this dissertation. The mathematical model takes into account both the drug dissolution and diffusion through the continuous matrices of the spherical microgels. Meshless Hermite-cloud method is employed to solve the formulated partial differential equations. The numerical simulating investigations of the drug delivery provide deeper insight into the drug release mechanisms and elucidate efficiently the influences of various physical parameters. Using this model, the drug diffusion coefficient and drug dissolution rate constant are identified numerically. The effects of several physical parameters on drug release are simulated and discussed in details, which include the microgel radius, drug saturation concentration, drug diffusion coefficient and drug dissolution rate constant.

1.4 Layout of dissertation

This dissertation is organized with six chapters, and a brief summary for each chapter is given as follows.

Chapter 1, Introduction, briefly gives the background of the present studies. The hydrogel is defined first with description of the formation and distinctive characteristics of hydrogels. Then a literature survey is made on the research history

and the applications, in which more attentions are centered on the temperature-stimulus-responsive hydrogels and the microgel-based drug delivery systems. Finally, the objectives and scopes of the present work are presented, followed by the layout of the dissertation.

Chapter 2, A Steady-State Model for Swelling Equilibrium of Thermo-Sensitive Hydrogels, develops a Multi-Effect-Coupling thermal-stimulus (MECtherm) model, based on the overview of the existing mathematic models and several theoretical considerations, for simulations of volume phase transition of the thermal-stimulus-responsive hydrogels immersed in solution with varying temperature. Then, non-dimensional implementation is produced to facilitate numerical computations.

Chapter 3, A Novel Meshless Technique: Hermite-Cloud Method, provides a numerical tool to solve the presently developed models consisting of linear/nonlinear partial differential equations, which includes a brief overview of meshless numerical techniques and numerical examinations.

Chapter 4, Numerical Simulation for Swelling Equilibrium of Thermo-Sensitive Hydrogels, uses the Hermite-cloud method to discretize and solve the developed MECtherm governing equations, and then compares the computational results with the experimental data. After validation of the MECtherm model, several parameter studies are made to discuss their effects on the swelling equilibrium of the thermo-sensitive hydrogels, including the fixed charge density, bathing solution concentration, effective crosslink density and initial polymer volume fraction.

Chapter 5, Transient Model Development for Simulation of Drug Delivery from Microgels, makes the study of drug delivery system. The controlled nifedipine release from microgels is simulated numerically with a mathematical model, which takes into account both the drug dissolution and diffusion through the continuous

matrices of the spherical microgels. The effects of several important physical parameters on drug release are evaluated in this chapter.

In Chapter 6, Conclusions and Future Works, several important conclusions are drawn from the present discussions and studies mentioned above, followed by the briefly recommended studies for future works.

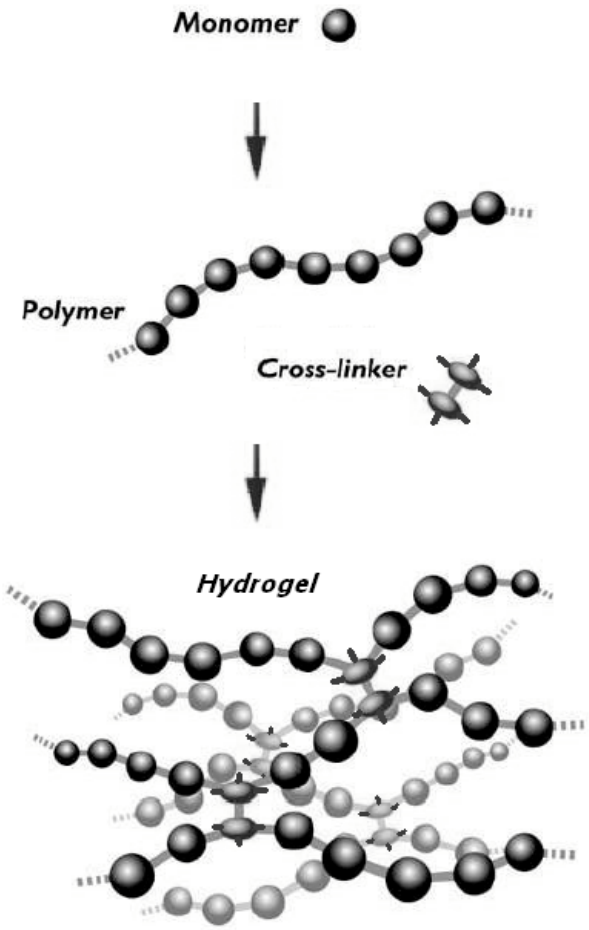

Figure 1.1 The forming process of hydrogels. The open circles denote monomers, solid lines denote polymer chains, and closed ellipses represent crosslink.

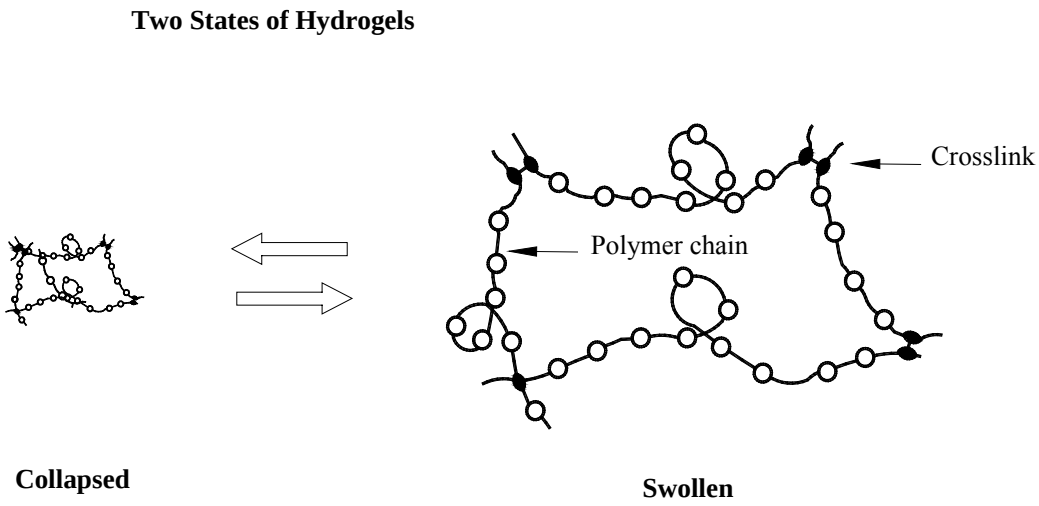

Figure 1.2 Schematic representation of hydrogels in collapsed and swollen states.

Chapter 2

A Steady-State Model for Swelling Equilibrium of Thermo-Sensitive Hydrogels

In this chapter, after a brief survey of the existing mathematic models and analysis of the fundamental interactions during the swelling and shrinking of the ionized hydrogels, a novel multiphysical mathematical model, consisting of a transcendental equation and the nonlinear coupled Poisson-Nernst-Planck partial differential equations, termed the Multi-Effect-Coupling thermal-stimulus (MECtherm) model, is developed for simulation of the volume phase transition of ionized temperature-sensitive hydrogels in swelling equilibrium state. Then non-dimensional implementation is presented to facilitate the computational performance, and followed by an illustration of the computational flow chart.

2.1 A brief background of existing mathematical models

As mentioned above, many studies were carried out in past decades for the thermal-stimulus-responsive hydrogels. However, most of them are experiment-based, few works involve mathematically modeling and simulation of the responsive behavior of the hydrogels, especially for the ionized hydrogels. They include the Lele et al.'s (1995) statistical thermodynamic model with consideration of hydrogen bond interaction for prediction of the swelling equilibrium of PNIPA hydrogel-water system. Otake et al. (1989) presented their model with effects of hydrophobic hydration and interaction for the thermally induced discontinuous shrinkage of ionized hydrogels. For the discontinuous volume phase transition, Erman and Flory

(1986) made the assumption that the polymer-solvent interaction parameter depends on the volume fraction of solid-phase polymer network. Recently, Hino and Prausnitz (1998) proposed a molecular thermodynamic model with combination of the impressible lattice-gas model (Birshtein and Pryamitsyn, 1991) and the interpolated affine model (Wolf, 1984) for simulation of the volume phase transition of PNIPA hydrogels. However, it is still difficult for these models to fit well with experimental data, and they provided only the qualitative prediction of volume phase transition of temperature sensitive hydrogels.

2.2 Development of Multi-Effect-Coupling thermal-stimulus (MECtherm) model

In this section, a multi-physic model with chemo-electro-thermo-mechanical coupling, called the Multi-Effect-Coupling thermal-stimulus (MECtherm) model, is developed mathematically to simulate the variations of volume phase transition with the temperature, mobile ion concentrations and electric potential for the swelling equilibrium of thermal-stimulus responsive hydrogels when immersed in solution. The present model incorporates the steady-state Nernst-Planck equation simulating the distribution of diffusive ionic species and the Poisson equation simulating the electric potential.

2.2.1 Theoretical considerations

In order to determine the volume phase transition of ionized temperature-sensitive hydrogels, usually we need to investigate four fundamental interactions, namely hydrogen bond, hydrophobic, electrostatic and the van der Waals interactions

(Shirota, 1998). The competitive balance between the repulsive and attractive interactions results in the volume phase transition (Li and Tanaka, 1992). According to the Flory's mean field theory (Flory, 1953) for swelling equilibrium of hydrogels, the above interactions for the volume phase transition of temperature-sensitive hydrogels can be presented mathematically in the form of three contributions to the change of free energy, namely polymer-solvent mixing, elastic deformation of the solid-phase polymer network and the osmotic pressure due to the gradients of ionic concentrations. Polymer-solvent mixing contributes to either attractive or repulsive forces, depending upon the relation between entropy change and the heat associated with the mixing. The elastic deformation of hydrogels is balanced by the mechanical elastic restoring force of solid-phase network due to the polymer elasticity. As one of driving expansion forces, the osmotic pressure is generated by the concentration difference of mobile ions between interior hydrogels and exterior solution. It is noted that the charged groups attached to the polymer chains play an essential role in the volume phase transition of the ionized hydrogels (Tanaka et al., 1980). When the hydrogels are immersed in the electrolyte solution, as illustrated in Figure 2.1 (Flory, 1953), the negatively charged groups attached to the polymer chains are compensated by the diffusive cations from the solution into the hydrogels, and consequently the cation concentration increases within the hydrogel prior to the volume change. This unequal distribution of the solute induces the osmotic pressure to drive the swelling of the ionic hydrogels. As a result, the volume phase transition of thermal-stimulus responsive hydrogels can be generally predicted by the thermodynamic equilibrium theorem. In the developed mathematic model, these three fundamental contribution forces to the swelling equilibrium are considered, and two forms of the polymer-solvent interaction parameters are employed.

2.2.2 Formulation of MECtherm governing equations

2.2.2.1 Free energy

From the thermodynamic viewpoint, the swelling equilibrium of ionized temperature-stimulus-responsive PNIPA hydrogels is determined by the final temperature field and the initial conditions including initial temperature, fixed charge density, the effective crosslink density, and the polymer-network volume fraction. Based on the Flory's mean field theory (Flory, 1953), the total change ΔG_{gel} of free energy within the ionized thermal-sensitive hydrogels may be expressed as

$$\Delta G_{gel} = \Delta G_{Mixing} + \Delta G_{Elastic} + \Delta G_{Ion}, \tag{2.1}$$

where ΔG_{Mixing}, $\Delta G_{Elastic}$ and ΔG_{Ion} represent the mixing, elastic deformation and ionic contributions to the change of free energy, respectively. By differentiating equation (2.1) with respect to the number of solvent molecules, the chemical potential of the solvent within the swollen hydrogels is obtained as

$$\Delta \mu_{gel} = \Delta \mu_{Mixing} + \Delta \mu_{Elastic} + \Delta \mu_{Ion}. \tag{2.2}$$

When swelling equilibrium is reached, the chemical potential of the solvent within the hydrogels equals to that of the solvent in the surrounding solution, namely

$$\Delta \mu_{Mixing} + \Delta \mu_{Elastic} + \Delta \mu_{Ion} - \Delta \mu_{Ion}^{*} = 0, \tag{2.3}$$

where $\Delta \mu_{Ion}^{*}$ represents the chemical potential of solvent in the external solution.

By the Flory-Huggins lattice theory (Flory, 1953), the change of mixing chemical potential induced by changing the solvent-solvent contact into solvent-polymer contact may be written as

$$\Delta \mu_{Mixing} = k_B T \upsilon^{-1} (\phi + \ln(1-\phi) + \chi \phi^2), \tag{2.4}$$

where k_B is Boltzmann constant, T is the absolute temperature, υ is the molar volume of the solvent, ϕ is the polymer-network volume fraction at swelling equilibrium state, and χ is the polymer-solvent interaction parameter.

It is known that the interaction parameter χ depends not only on the absolute temperature T, but also on the polymer-network volume fraction ϕ (Moerkerke et al., 1995; Shirota et al., 1998; Hino and Prausnitz, 1998). In the case of swollen hydrogels with lower polymer-network volume fraction below the lower critical solution temperature (LCST), we employ the polymer-solvent interaction parameter in the following form as

$$\chi = \chi_1(T) + \chi_2\phi = (\delta h - \delta s T)/(k_B T) + \chi_2\phi, \tag{2.5}$$

in which χ_2 is an experimentally adjustable parameter. δs and δh are the changes of entropy and enthalpy per monomeric unit of the network, respectively. The numerical studies in this dissertation will validate that the parameter χ expressed by equation (2.5) is suitable for simulation of the PNIPA hydrogels at swelling state. Furthermore, in the case of shrunken hydrogels with higher volume fraction of polymer-network above LCST, the interaction parameter χ is defined by

$$\chi = F(T)P(\phi), \tag{2.6}$$

where $F(T)$ and $P(\phi)$ are the functions of absolute temperature and polymer-network volume fraction, respectively. $P(\phi)$ given by Bae et al. (1993) is

$$P(\phi) = (1 - b\phi)^{-1}, \tag{2.7}$$

in which b is an empirical parameter, and it is taken to be 0.65 in this dissertation. For $F(T)$, we have the expression given by Hino and Prausnitz (1998)

$$F(T)=\frac{z}{2}\left(\frac{\zeta+2\zeta_{12}}{RT}+2\ln\left(\frac{1+s_{12}}{1+s_{12}\exp(\zeta_{12}/(RT))}\right)\right), \tag{2.8}$$

where z is the lattice coordination number (z=6), ζ is the interchange energy, ζ_{12} is the difference between the segmental interaction energy for specific interactions and that for non-specific interactions, R is the gas constant, and s_{12} is the degeneracy ratio of non-specific interactions to that of specific interactions. In addition, it is also noted that, in numerical implementation, the transformation between equations (2.5) and (2.6) is determined by detecting the volume phase transition, when the difference of polymer volume fractions between the previous and current iterating steps is much larger than the specified convergence region.

In order to present the contribution of elastic deformation to the change of chemical potential, the affine model is given by Flory (1953) as

$$\Delta\mu_{Elastic}=k_BTv_e((\phi/\phi_0)^{1/3}-(\phi/2\phi_0)), \tag{2.9}$$

where v_e is the effective crosslink density, ϕ_0 is the initial polymer-network volume fraction in the pregel solution, and ϕ_0/ϕ is the volume swelling ratio.

For the ionic contribution to the change of chemical potential, usually it is determined by the concentration difference between the mobile ions inside and outside the hydrogels (Flory, 1953) as

$$\Delta\mu_{Ion}-\Delta\mu^*_{Ion}=-k_BT\sum_{j=1}^{N}(c_j-c_j^*), \tag{2.10}$$

where n denotes the number of different mobile ion species, c_j and c_j^* are the jth mobile ion concentrations in the interior hydrogels and exterior bathing solution, respectively.

By substituting equations (2.4), (2.9) and (2.10) into equation (2.3), the swelling equilibrium governing equation is obtained in the following transcendental equation form

$$\upsilon^{-1}(\phi + \ln(1-\phi) + \chi\phi^2) + v_e((\phi/\phi_0)^{1/3} - (\phi/2\phi_0)) - \sum_{j=1}^{N}(c_j - c_j^*) = 0 . \qquad (2.11)$$

When the hydrogels are immersed into pure water, where the mobile ion concentrations of the external solution are equal to zero, equation (2.11) can be simplified into the transcendental equation as

$$\upsilon^{-1}(\phi + \ln(1-\phi) + \chi\phi^2) + v_e((\phi/\phi_0)^{1/3} - (\phi/2\phi_0)) - c_f^0\phi/2\phi_0 = 0 . \qquad (2.12)$$

where c_f^0 is the fixed-charge density at the reference state ($\phi = \phi_0$).

2.2.2.2 Poisson-Nernst-Planck theory

In order to couple the effects of mobile ion concentrations and electric potentials in simulation of temperature-sensitive hydrogels, Poisson-Nernst-Planck formulation is required. If the contributions of migration and diffusion to the transport of mobile ions are considered only during the thermal swelling of hydrogels, the steady-state Nernst-Planck equation for the *j*th ion can be expressed by (Samson et al., 1999)

$$D_j\nabla^2 c_j + \frac{FD_j z_j}{RT}\left(\nabla c_j \nabla\psi + c_j\nabla^2\psi\right) = 0 \qquad (j = 1,2,\cdots N) \qquad (2.13)$$

where F is the Faraday constant, D_j is the diffusive coefficient, z_j is the valence of the *j*th mobile ion, c_j is the concentration of the *j*th mobile ion, and ψ is the electric potential.

For the relation between the mobile ion concentration and the electric potential, the Poisson equation (Samson et al., 1999) is required as

$$\nabla^2\psi = -\frac{F}{\varepsilon\varepsilon_0}\left(z_f c_f + \sum_{j=1}^{N}(z_j c_j)\right), \tag{2.14}$$

where ε_0 is the permittivity for vacuum, ε is the dielectric constant of medium relative to vacuum (e.g. ε=80 for water), z_f is the valence of fixed charges, and c_f is the fixed-charge density.

In the simulation of ionized thermal-stimulus-responsive hydrogels, it is generally assumed that the fixed charges attached to the solid-phase polymer networks distribute uniformly within the hydrogel during thermal swelling, and the total amount of fixed charges is invariable. In other words, the fixed-charge density $c_f = c_f^0\phi/\phi_0$ in the swelling equilibrium state.

2.3 Numerical implementation

2.3.1 Reduced 1-D governing equations

For the isotropic swelling of the hydrogels, the elongation ratios along three principal axes are equal to each other, in which the displacement vector $\boldsymbol{u}$ may be expressed by the difference between the deformed position $\boldsymbol{x}(\alpha x_0, \alpha y_0 \alpha z_0)$ (here α is the linear volume swelling ratio, and $\alpha = (V/V_0)^{1/3} = (\phi_0/\phi)^{1/3}$) and original position $\boldsymbol{x_0}(x_0, y_0 z_0)$, namely

$$\boldsymbol{u} = \boldsymbol{x} - \boldsymbol{x_0} = ((\phi_0/\phi)^{1/3} - 1)\boldsymbol{x_0}. \tag{2.15}$$

In this dissertation, only the cylindrical hydrogels (Figure 2.2) are simulated numerically. Due to axis-symmetry therefore, it is reasonable to use one-dimensional computational domain along the radial direction covering both the hydrogel radius and bathing solution, as shown in Figure 2.3. The steady-state Nerst-Planck equation in the polar coordinates is thus simplified as

$$\frac{\partial^2 c_j}{\partial r^2}+\frac{1}{r}\frac{\partial c_j}{\partial r}+\frac{Fz_j}{RT}\left(c_j\frac{\partial^2\psi}{\partial r^2}+\frac{c_j}{r}\frac{\partial\psi}{\partial r}+\frac{\partial c_j}{\partial r}\frac{\partial\psi}{\partial r}\right)=0 \qquad (j=1,2,\cdots N) \quad (2.16)$$

and the Poisson Equation is rewritten as

$$\frac{\partial^2\psi}{\partial r^2}+\frac{1}{r}\frac{\partial\psi}{\partial r}=-\frac{F}{\varepsilon\varepsilon_0}\left(z_f c_f+\sum_{j=1}^{N}(z_j c_j)\right). \quad (2.17)$$

The radial displacement of the deformed hydrogel is given as

$$u_r=((\phi_0/\phi)^{1/3}-1)R_0, \quad (2.18)$$

where R_0 is the radius of cylindrical hydrogel at the reference state.

Correspondingly, the required boundary conditions are applied at both the ends of 1-D computational domain, as shown in Figure 2.3. Due to axisymmetry of the present problem, the boundary conditions at the end point O of the circle centre are given as

$$\frac{\partial\psi}{\partial r}=0 \quad \text{and} \quad \frac{\partial c_j}{\partial r}=0 \quad (j=1,2,\cdots N) \quad \text{at } r=0 \quad (2.19)$$

The boundary conditions at the end point B of the solution region are given by

$$\psi=0 \quad \text{and} \quad c_j=c^* \quad (j=1,2,\cdots N) \quad \text{at } r=L \quad (2.20)$$

2.3.2 Non-dimensional implementation

To facilitate the numerical implementation of the models developed above, a set of non-dimensional variables is defined. They are non-dimensional radius

$\xi = r/L_{ref}$, non-dimensional concentration of the *j*th ionic species $\overline{c_j} = c_j/c_{ref}$, non-dimensional fixed charge density $\overline{c_f} = c_f/c_{ref}$, and non-dimensional electrical potential $\overline{\psi} = (F\psi)/(\eta RT)$, in which L_{ref}, c_{ref} and ψ_{ref} are the given reference parameters.

After substituting the above non-dimensional formulations to equations (2.16) and (2.17), the non-dimensional steady-state Poisson-Nernst-Planck system is finally obtained as

$$\frac{\partial^2 \overline{c_j}}{\partial \xi^2} + \frac{1}{\xi}\frac{\partial \overline{c_j}}{\partial \xi} + \eta z_j \left(\overline{c_j} \frac{\partial^2 \overline{\psi}}{\partial \xi^2} + \frac{\overline{c_j}}{\xi}\frac{\partial \overline{\psi}}{\partial \xi} + \frac{\partial \overline{c_j}}{\partial \xi}\frac{\partial \overline{\psi}}{\partial \xi} \right) = 0 \qquad (j = 1,2,\cdots N) \quad (2.21)$$

$$\frac{\partial^2 \overline{\psi}}{\partial \xi^2} + \frac{1}{\xi}\frac{\partial \overline{\psi}}{\partial \xi} = -\frac{F^2 L_{ref}^2 c_{ref}}{\varepsilon \varepsilon_0 \eta RT} \left(z_f \overline{c_f} + \sum_{j=1}^{N} (z_j \overline{c_j}) \right) \quad (2.22)$$

2.3.3 Computational flow chart

For simulation of response behavior of the ionized thermo-sensitive hydrogels when immersed in univalent electrolyte solution, we need solve iteratively a set of coupled nonlinear partial differential governing equations, consisting of the swelling equilibrium equation (2.11), Nernst-Plank equation (2.21) and Poisson equation (2.22). Firstly, a guessed value of polymer-network volume fraction ϕ^* at a given temperature T is provided. Using the Newton's iterative technique for solution of the coupled nonlinear partial differential equations (2.21) and (2.22), the distributions of the electric potential and mobile ion concentrations are computed at this temperature. Subsequently, substituting the computed ionic concentrations into the swelling equilibrium equation (2.11), the corresponding volume fraction ϕ of the polymer network is obtained, and then used as the guessed value ϕ^* in next iterative step. In

this way, the iterative recurrence is conducted until the convergence of polymer network volume fraction. A corresponding computational flow chart is illustrated in Figure 2.4.

In summary, the multiphysical model with chemo-electro-thermo-mechanical coupling has been developed, and termed the Multi-Effect-Coupling thermal-stimulus (MECtherm) model. It consists of the nonlinear coupled Poisson-Nernst-Planck partial differential equations (2.13) and (2.14) and the transcendental equation (2.11) of the swelling equilibrium based on the Flory's mean field theory. The model has the capability of simulating the volume phase transition of the ionized temperature-stimulus-responsive hydrogels when they are immersed in the bathing solution with temperature change. This model will be validated in Chapter 4, and the influences of several important physical parameters and material properties will also be simulated and discussed in detail.

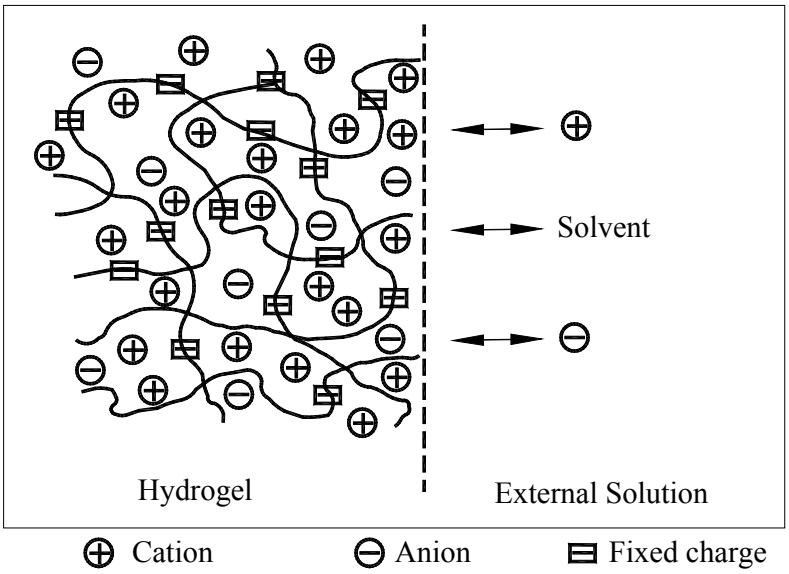

Figure 2.1 A schematic diagram of the microscopic structure of the thermo-sensitive ionized PNIPA hydrogel in electrolyte solution (Flory, 1953).

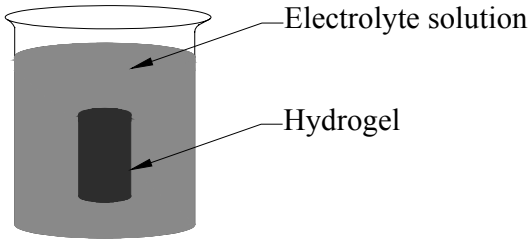

Figure 2.2 Schematic diagram of a thermo-sensitive ionized cylindrical PNIPA hydrogel immersed in electrolyte solution.

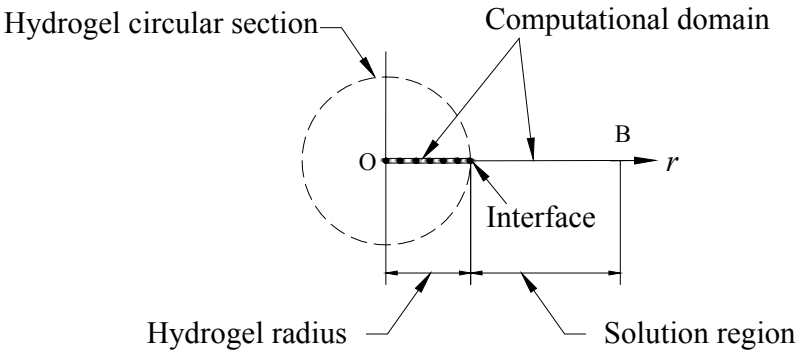

Figure 2.3 One-dimensional computational domain along the radial direction covers both the hydrogel and bathing solution.

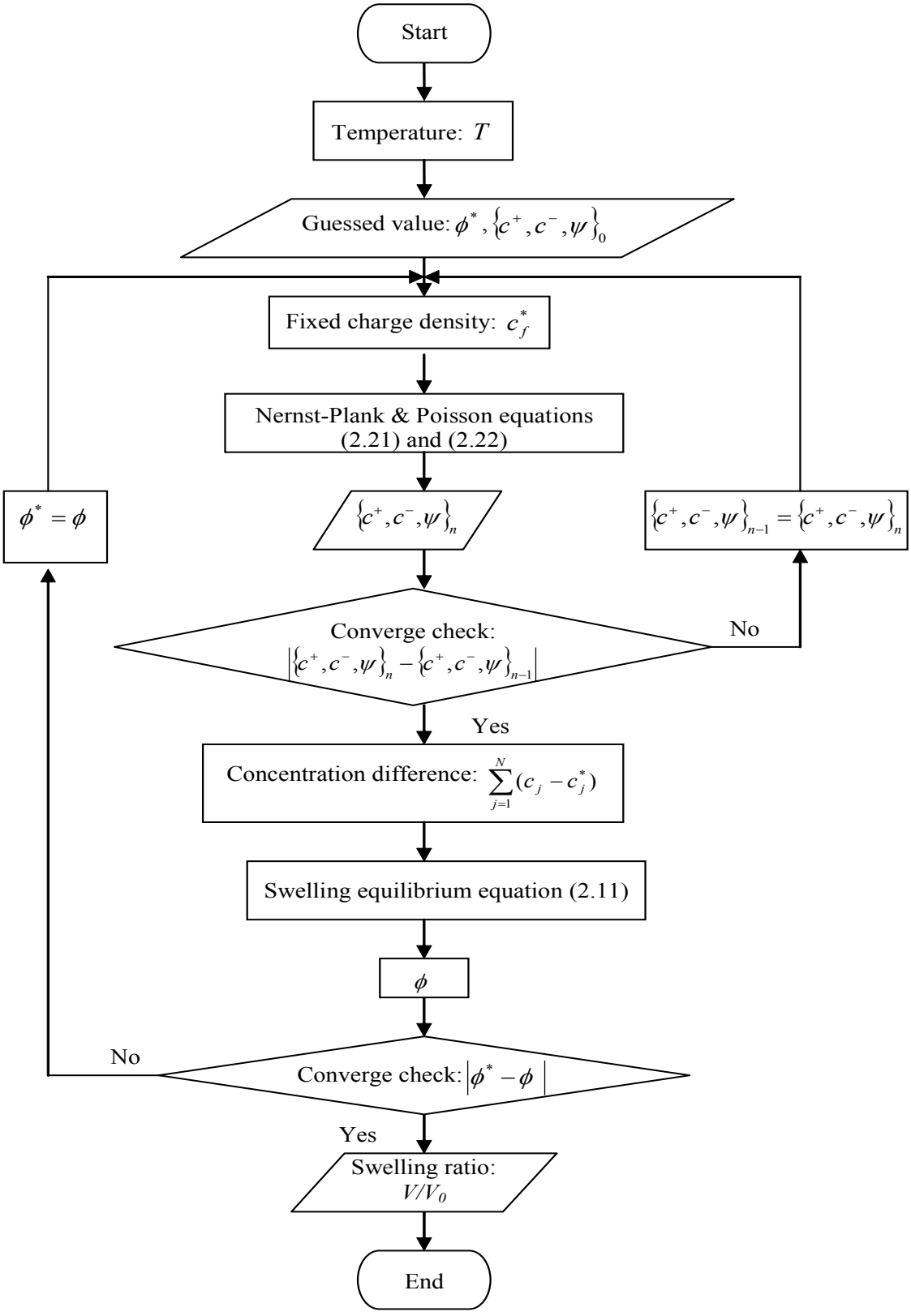

Figure 2.4 Computational flow chart.

Chapter 3

A Novel Meshless Technique: Hermite-Cloud Method

In this chapter, as a novel true meshless numerical technique, Hermite-cloud method is presented, which will be employed as numerical tool to solve the present differential boundary value problems. This method uses the Hermite interpolation theorem for construction of the interpolation functions, and the point collocation technique for discretization of the partial differential equations. Numerical examinations show that the computational accuracy of Hermite-cloud method is quite acceptable.

3.1 A brief overview of meshless numerical techniques

A growing interest has emerged in the development of meshless methods for numerical solution of partial differential equations (PDEs) in recent years. Meshless methods use only a set of scattered nodes representing the problem domain, and don't require the connectivity information among the scattered nodes. This makes the methods be different from the traditional numerical approaches such as the finite element method (FEM). Using the FEM, a problem domain is required to be divided into small elements and the field function is approximated within each element through simple interpolation functions. Although FEM has wide range of engineering and science applications, it still has some inherent shortcomings. First, large distortion of element is not allowed. If the element is heavily distorted, shape functions for this element are of poor quality and thus the numerical results may not be acceptable

(Belytschko et al., 1996). Second, the computational cost is very high in creating meshes. The cost of mesh generation for complex geometry is very significant and could be more expensive than solving the problem. In addition, it is difficult to implement adaptive scheme, where remeshing process is required for the FEM to ensure the nodal connectivity properly defined at each adaptive step. This inevitable process becomes the burden of computation as mesh generation could be very expensive. In order to overcome the shortcomings, the meshless methods are developed. Usually they save computation time because the mesh generation is not required. Relatively, they can easily solve large deformation and strong nonlinear problems, since the connectivity among the nodes is generated as part of the computation and can change with time. Moreover, they can easily solve problems with multi-domains and multi-physics requirement. Thus, meshless methods have potential applications in adaptive techniques, especially in emerging technologies such as micro-electro-mechanical-systems (MEMS). The presently developed Hermite-cloud method, which constructs the shape functions corresponding to the unknown functions and their first-order derivatives respectively, improves the computational accuracy at the scattered discrete points in the domain not only for approximate solutions but also for their first-order derivatives. It is a very efficient numerical technique for solutions of the partial differential boundary value (PDBV) problems with high gradient solution field (Li et al., 2003). Therefore, it is used here for solving the hydrogel problems discussed in previous chapters, where the iteration implementation for solving the nonlinear coupled partial differential governing equations requires the remeshing process in both the domains of the hydrogels and surrounding solution, and high concentration gradient always occurs at the interfaces between the hydrogels and surrounding solution.

So far many meshless methods have been proposed (Liu GR, 2002). One can generally classify these meshless approaches into two groups, depending on the requirement of integration or not (Liu GR, 2002), or depending on computational modeling (Li and Liu WK, 2002). The first is based on the PDEs with strong-form, and the second is based on the PDEs with weak-form. Furthermore, the meshless weak-strong (MWS) form method has also been developed, which combines the strong-form with weak-form of partial differential boundary value problems.

In the first group of strong-form meshless methods, the collocation technique is usually used to discretize the PDEs at nodes. This group includes the generalized finite difference method (Perrone and Kao, 1975; Liszka, 1984), the smooth particle hydrodynamics (SPH) (Gingold and Monaghan, 1977; Monaghan, 1985; Benz, 1990), the finite point method (Onate et al., 1996), the hp-meshless cloud method (Liszka et al., 1996) and the collocation method (Franke and Schaback, 1997; Liu Xin et al., 2002; Zhang et al., 2001). These methods do not use any mesh for both field variable approximation and integration, and are simple to implement and computationally efficient (Liu GR and Gu, 2004). They have been successfully applied in computational mechanics, particularly in fluid mechanics. Nevertheless, these methods have the shortcomings, such as, the unstable computation and less accuracy, especially for PDEs with Neumann boundary conditions.

The second group of weak-form meshless methods includes the use of global weak-form and local weak-form of PDEs. The examples based on the global weak-form include the diffuse element method (Nayroles et al., 1992), the element-free Garlerkin (EFG) method (Belytschko et al., 1994-1997), the reproducing particle method (RKPM) (Liu WK et al., 1995-1997) and the point interpolation method

(PIM) (Liu GR and Gu, 2001a, 2004; Gu and Liu GR, 2002, 2003a). The examples based on the local weak-form include the meshless Petrov-Galerkin method (MLPG) (Atluri and Zhu, 1998, 2000; Atluri and Shen, 2002; Atluri et al., 1999a, b; Gu and Liu GR, 2001a, b) and the family of local point interpolation method (LPIM) (Gu and Liu GR, 2001c; Liu GR and Gu, 2001b, c, 2002). These weak-form meshless techniques have many advantages, such as good computational stability and excellent accuracy, since the weak form can minish the error over the integral domain and control the error level. Furthermore, the weak form can naturally satisfy the Neumann boundary conditions. As such, they have been successfully used in solid mechanics. However, these methods are not "truly" meshless, when compared with the common finite element method, they are only "meshless" in terms of the interpolation of the field variables.

Moreover, some other types of meshless methods have also been proposed. For example, there are the boundary node method (BNM) (Mukherjee YX and Mukherjee S, 1997), the boundary point interpolation method (Gu and Liu GR, 2002, 2003a), and so on. Some methods with combination of two meshless methods, or combing a meshless method with a conventional method, have also been developed, such as, the EFG/FEM, EFG/BEM/HBEM, MLPG/BEM/FEM (Hegen, 1996; Liu GR and Gu, 2000b; Gu and Liu GR, 2001d; Gu and Liu GR, 2003b).

In brief, the meshless numerical methods are able to avoid the disadvantages of traditional numerical techniques, e.g. the finite element method. Therefore, they have very good potential applications in simulations of multiphysical problems.

3.2 Hermite-cloud method

The numerical technique employed in this dissertation is the true meshless Hermite-cloud method (Li et al., 2003). This method uses the Hermite interpolation theorem for the construction of the interpolation functions, and the point collocation technique for discretization of the partial differential equations. This technique is based on the classical reproducing kernel particle method except that a fixed reproducing kernel approximation is employed instead. As a true meshless technique, the present method constructs the Hermite-type interpolation functions to directly compute the approximate solutions of both the unknown functions and the first-order derivatives. The necessary auxiliary conditions are also constructed to generate a complete set of partial differential equations with mixed Dirichlet and Neumann boundary conditions. The point collocation technique is then used for discretization of the governing partial differential equations.

Using the Hermite-cloud method, the approximation $\widetilde{f}(x)$ of a one-dimensional unknown real function $f(x)$ can be constructed by

$$\widetilde{f}(x) = \sum_{n=1}^{N_T} N_n(x) f_n + \sum_{m=1}^{N_S} (x - \sum_{n=1}^{N_T} N_n(x) x_n) M_m(x) g_{xm}, \tag{3.1}$$

where N_T and $N_S (\le N_T)$ are the total numbers of scattered points, covering both the interior computational domain and the surrounding edges, for the point values f_n and g_{xm} respectively. f_n is the point value of unknown real function $f(x)$ at the *n*th point, and g_{xm} is the point value of the first-order differential, $g_x(x) = df(x)/dx$, at the *m*th point. The corresponding discrete approximation is written as

$$\widetilde{g}_x(x) = \sum_{m=1}^{N_S} M_m(x) g_{xm}, \tag{3.2}$$

In equation (3.1), the shape function $N_n(x)$ and $M_m(x)$ for the respective functions $f(x)$ and $g_x(x)$ are defined as (Ng et al., 2003)

$$N_n(x) = \boldsymbol{B}(u_n)\boldsymbol{A}^{-1}(x_k)\boldsymbol{B}^T(x)K(x_k - u_n)\Delta L_n, \qquad n = 1,2,\ldots,N_T \tag{3.3}$$

$$M_m(x) = \widetilde{\boldsymbol{B}}(u_m)\widetilde{\boldsymbol{A}}^{-1}(x_k)\widetilde{\boldsymbol{B}}^T(x)K(x_k - u_m)\Delta L_m, \qquad m = 1,2,\ldots,N_S \tag{3.4}$$

in which ΔL_n and ΔL_m are defined as the cloud sizes of the *n*th and *m*th points respectively, i.e. the dilation parameters as defined by Liu et al (1995). The increase of the cloud sizes of the kernel function typically increases the number of points that contribute to the unknown value at the interest point *n* (Ohs and Aluru, 2001). It is also noted that generally the increase of node density definitely improve the computational accuracy. However, we can not blindly increase the radius of influence domain or support size of nodal shape function. Otherwise, computational cost increases evidently (Liu et al., 2003) and computational instability may occur (Tang et al., 2003). Furthermore, when a few points are used, the solution may be sensitive to the number of points included in each cloud and this may cause distortion of the results, especially in the boundary areas (Ohs and Aluru, 2001). The selection of the dilation parameters should correspond to some local information to match the resolution of the given sampling points (Liu et al., 1995). According to our computing experience, usually $\Delta L_n = \Delta L_m = 1.17\Delta x$ is good enough for equidistance point distributions in the present simulations of the responsive hydrogels, in which Δx refers to the spacing between points in *x*-direction.

$\boldsymbol{B}(u)$ and $\widetilde{\boldsymbol{B}}(u)$ are the linearly independent basis-function vectors which are given by

$$\boldsymbol{B}(u) = \{b_1(u),\ b_2(u),\ b_3(u)\} = \{1,\ u,\ u^2\}, \tag{3.5}$$

$$\widetilde{\boldsymbol{B}}(u) = \{b_1(u),\ \ b_2(u)\} = \{1,\ \ u\}, \tag{3.6}$$

and $\boldsymbol{A}(x_k)$ and $\widetilde{\boldsymbol{A}}(x_k)$ are symmetric constant matrices associated with the central point x_k of the fixed cloud,

$$A_{ij}(x_k) = \sum_{n=1}^{N_T} b_i(u_n) K(x_k - u_n) b_j(u_n) \Delta L_n \text{ ,} \qquad (i, j = 1,\ \ 2,\ \ 3) \tag{3.7}$$

$$\widetilde{A}_{ij}(x_k) = \sum_{m=1}^{N_S} b_i(u_m) K(x_k - u_m) b_j(u_m) \Delta L_m \text{ ,} \qquad (i, j = 1,\ \ 2) \tag{3.8}$$

where $K(x_k - u)$ is a kernel function constructed by cubic spline function as,

$$K(x_k - u) = \frac{1}{\Delta L_k} \begin{cases} 0 & 2 < z \\ (2-z)^3 / 6 & 1 \le z \le 2 \\ (2/3) - z^2 (1 - z/2) & 0 \le z \le 1 \end{cases}, \tag{3.9}$$

where $z = \left|(x_k - u)\right| / \Delta L_k$.

Due to the additionally introduced unknown function $g_x(x)$, the auxiliary condition is required in order to implement the Hermite-cloud method. Imposing the first-order partial differential with respect to x on the approximation $\widetilde{f}(x)$ expressed by equation (3.1), and noting equation (3.2), the auxiliary condition is derived as

$$\sum_{n=1}^{N_T} N_{n,x}(x) f_n - \sum_{m=1}^{N_S} \left(\sum_{n=1}^{N_T} N_{n,x}(x) x_n \right) M_m(x) g_{xm} = 0, \tag{3.10}$$

where $N_{n,x}(x)$ denotes the first derivative of $N_n(x)$ with respect to the variable x.

3.3 Numerical implementation

The formulation of the present Hermite-cloud method has been completed in the previous section, and it is able to solve generic engineering partial differential boundary value (PDBV) problems, such as,

$$Lf(x) = P(x), \qquad \text{PDEs in computational domain } \Omega \tag{3.11}$$

$$f(x) = Q(x), \qquad \text{Dirichlet boundary condition on } \Gamma_D \tag{3.12}$$

$$\partial f(x)/\partial n = R(x), \qquad \text{Neumann boundary condition on } \Gamma_N \tag{3.13}$$

where L is differential operator and $f(x)$ an unknown real function. By using the point collocation technique, the approximation of the above PDBV problem can be expressed in the follow discrete forms as

$$L\widetilde{f}(x_j) = P(x_j), \qquad (j = 1,2,\ldots,N_\Omega) \tag{3.14}$$

$$\widetilde{f}(x_j) = Q(x_j), \qquad (j = 1,2,\ldots,N_D) \tag{3.15}$$

$$\partial\widetilde{f}(x_j)/\partial n = R(x_j), \quad (j = 1,2,\ldots,N_N) \tag{3.16}$$

where N_Ω, N_D and N_N are the numbers of scattered points in the interior computational domain and along the Dirichlet and Neumann edges, respectively. Thus total number of scattered points $N_T = N_\Omega + N_D + N_N$.

Substituting equations (3.1) and (3.2) into equations (3.14)-(3.16) and considering the auxiliary condition (3.10), a set of discrete algebraic equations with respect to unknown point values f_i and g_{xi} is derived in the following matrix form as

$$[H_{ij}]_{(N_T+N_S)\times(N_T+N_S)}\{F_i\}_{(N_T+N_S)\times 1} = \{d_i\}_{(N_T+N_S)\times 1}, \tag{3.17}$$

where $\{d_i\}$ and $\{F_i\}$ are $(N_T + N_S)$-order column vectors

$$\{F_i\}_{(N_T+N_S)\times 1} = \{\{f_i\}_{1\times N_T}, \{g_{xi}\}_{1\times N_S}\}^T, \tag{3.18}$$

$$\{d_i\}_{(N_T+N_S)\times 1} = \{\{P(x_i)\}_{1\times N_\Omega}, \{Q(x_i)\}_{1\times N_D}, \{R(x_i)\}_{1\times N_N}, \{0\}_{1\times N_S}\}^T, \tag{3.19}$$

and $[H_{ij}]$ is a $(N_T + N_S)\times(N_T + N_S)$ coefficient matrix

$$[H_{ij}] = \begin{bmatrix} [LN_j(x_i)]_{N_\Omega \times N_T} & [L((x_i - \sum_{n=1}^{N_T} N_n(x_i)x_n)M_j(x_i))]_{N_\Omega \times N_S} \\ [N_j(x_i)]_{N_D \times N_T} & [0]_{N_D \times N_S} \\ [0]_{N_N \times N_T} & [M_j(x_i)]_{N_N \times N_S} \\ [N_{j,x}(x_i)]_{N_S \times N_T} & [(-\sum_{n=1}^{N_T} N_{n,x}(x_i)x_n)M_j(x_i)]_{N_S \times N_S} \end{bmatrix}. \quad (3.20)$$

By solving numerically the set of linear algebraic equations (3.17), $(N_T + N_S)$ point values $\{F_i\}$ are obtained. Accordingly, the approximate solutions $\widetilde{f}(x)$ and the first-order differential $\widetilde{g}_x(x)$ can be computed through equations (3.1) and (3.2), respectively.

3.4 Numerical Validation

For examination of the Hermite-cloud method, two examples of differential boundary value problems with exact solutions are taken below.

The first example is a Poisson equation with a forcing term as a function of x. The governing equation and boundary conditions are written as

$$\frac{\partial^2 u}{\partial x^2} = \frac{105}{2}x^2 - \frac{15}{2}, \quad (-1 < x < 1) \quad (3.21)$$

$$u = 1 \qquad at \quad x = -1 \quad , \quad (3.22)$$

$$\frac{\partial u}{\partial x} = 10 \qquad at \quad x = 1. \quad (3.23)$$

The exact solution of this Poisson problem is given as

$$u = \frac{35}{8}x^4 - \frac{15}{4}x^2 + \frac{3}{8}. \quad (3.24)$$

A comparison of the numerical results by the Hermite-cloud method with the exact solution (3.24) is illustrated in Figure 3.1 for the Poisson boundary value

problem (3.21) to (3.23). It is observed that a very good agreement between the Hermite-cloud and exact results is achieved, in which the maximum relative discrepancy is 2.63% at x=0.66.

The second example with a high gradient in a local area is taken to see how the Hermite-cloud method performs. The corresponding differential governing equation and boundary conditions are written as

$$\frac{\partial^2 u}{\partial x^2} = -6x - \left[\frac{2}{\alpha^2} - 4\left(\frac{x-\beta}{\alpha^2}\right)^2\right]\exp\left[-\left(\frac{x-\beta}{\alpha^2}\right)^2\right], \quad (0 \le x \le 1) \tag{3.25}$$

$$u = \exp\left(-\frac{\beta^2}{\alpha^2}\right) \qquad at \quad x = 0 \tag{3.26}$$

$$\frac{\partial u}{\partial x} = -3 - 2\left(\frac{x-\beta}{\alpha^2}\right)\exp\left[-\left(\frac{1-\beta}{\alpha^2}\right)^2\right] \qquad at \quad x = 1 \quad . \tag{3.27}$$

The exact solution of this differential boundary value problem with local high gradient is given as

$$u = -x^3 + \exp\left[-\left(\frac{x-\beta}{\alpha}\right)^2\right]. \tag{3.28}$$

In the present numerical comparison, $\beta = 0.5$ and $\alpha = 0.05$ are taken. As shown in Figure 3.2, a high local gradient is generated near $x = 0.5$, and the numerical results of the Hermite-cloud method match well with the exact solution, in which the maximum relative discrepancy is 5.65% at x=0.56.

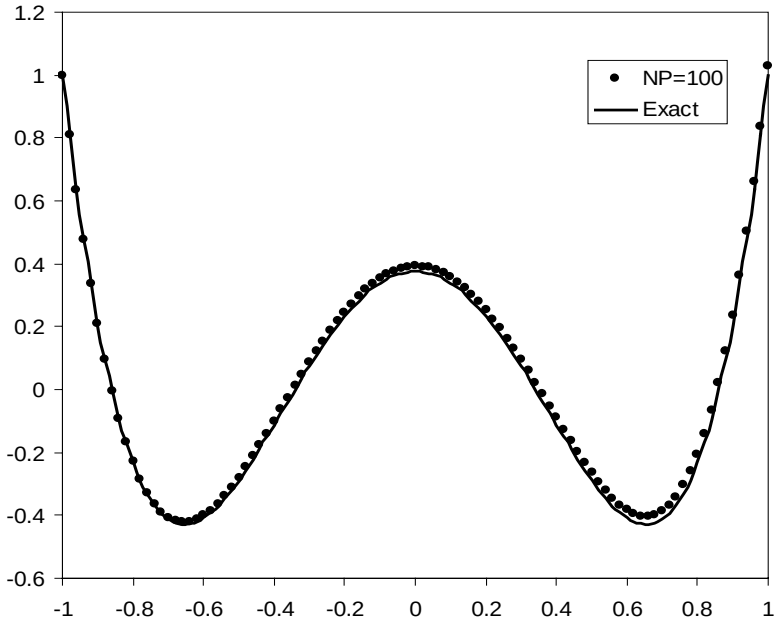

Figure 3.1 Comparison of computed Hermite-cloud results with the exact solution for the 1-D Poisson equation.

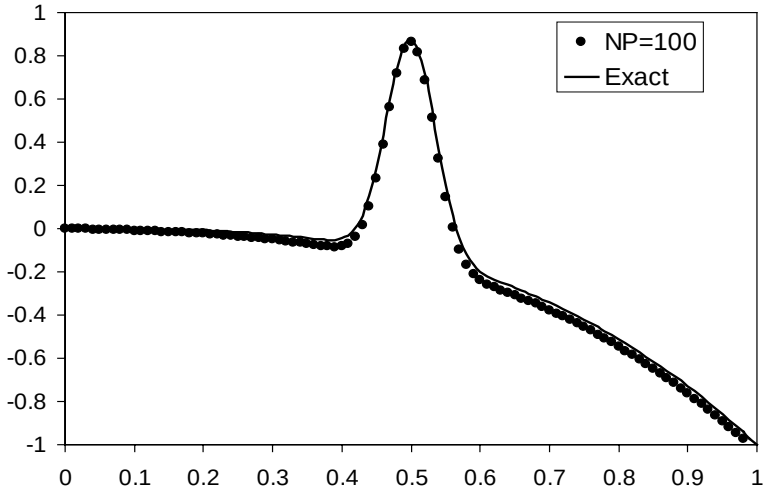

Figure 3.2 Comparison of computed Hermite-cloud results with the exact solution for the 1-D differential boundary value problem with a high local gradient.

Chapter 4

Numerical Simulation for Swelling Equilibrium of Thermo-Sensitive Hydrogels

In this chapter, the developed MECtherm governing equations are discretized and solved by the Hermite-cloud method for simulation of swelling equilibrium of temperature-sensitive hydrogels. The numerically computed results are compared with the experimental data from open literature to examine the present MECtherm model. Simulations are made for prediction of the influences of several physical parameters on the response behaviors of the hydrogels in the swelling equilibrium state when immersed in the solution with varying temperature. Detailed discussions are also carried out for the effect of temperature on the volume phase transition and the distributions of ionic concentrations, fixed charge density and electric potential.

4.1 Discretization of Poisson-Nernst-Plank equations

In order to simulate the steady-state swelling equilibrium of temperature-sensitive hydrogels, the non-dimensional Nernst-Plank equations (2.21) and Poisson equation (2.22) are discretized in spatial domain and then solved by the Hermite-cloud method.

According to the Hermite-cloud method, the approximations of non-dimensional unknown variables, $\overline{c_j}$ and $\overline{\psi}$, and their derivatives are given as

$$\overline{c_j} = \sum_{n=1}^{N_T} N_n(\xi_i)\overline{c_n^j} + \sum_{m=1}^{N_S}(\xi_i - \sum_{n=1}^{N_T} N_n(\xi_i)\xi_n)M_m(\xi_i)\overline{c_{\xi m}^j}, \tag{4.1}$$

$$\frac{\partial \overline{c_j}}{\partial \xi} = \sum_{m=1}^{N_S} M_m(\xi_i)\overline{c_{\xi m}^j}, \tag{4.2}$$

$$\frac{\partial^2 \overline{c_j}}{\partial \xi^2} = \sum_{n=1}^{N_T} N_{n,\xi\xi}(\xi_i)\overline{c_n^j}, \tag{4.3}$$

$$\overline{\psi} = \sum_{n=1}^{N_T} N_n(\xi_i)\overline{\psi}_n + \sum_{m=1}^{N_S}(\xi_i - \sum_{n=1}^{N_T} N_n(\xi_i)\xi_n)M_m(\xi_i)\overline{\psi}_{\xi m}, \tag{4.4}$$

$$\frac{\partial \overline{\psi}}{\partial \xi} = \sum_{m=1}^{N_S} M_m(\xi_i)\overline{\psi}_{\xi m}, \tag{4.5}$$

$$\frac{\partial^2 \overline{\psi}}{\partial \xi^2} = \sum_{n=1}^{N_T} N_{n,\xi\xi}(\xi_i)\overline{\psi}_n. \tag{4.6}$$

Substituting equations (4.1)-(4.6) into governing equations (2.21) and (2.22), the approximations of Poisson-Nernst-Planck system are written as

$$\begin{aligned}\sum_{n=1}^{N_T} N_{n,\xi\xi}(\xi_i)\overline{c_n^j} + \frac{1}{\xi_i}\sum_{m=1}^{N_S} M_m(\xi_i)\overline{c_{\xi m}^j} + \eta z_j \sum_{m=1}^{N_S} M_m(\xi_i)\overline{c_{\xi m}^j}\sum_{m=1}^{N_S} M_m(\xi_i)\overline{\psi}_{\xi m} + \\ + \eta z_j[\sum_{n=1}^{N_T} N_n(\xi_i)\overline{c_n^j} + \sum_{m=1}^{N_S}(\xi_i - \sum_{n=1}^{N_T} N_n(\xi_i)\xi_n)M_m(\xi_i)\overline{c_{\xi m}^j}]\times \\ \times[\sum_{n=1}^{N_T} N_{n,\xi\xi}(\xi_i)\overline{\psi}_n + \frac{1}{\xi_i}\sum_{m=1}^{N_S} M_m(\xi_i)\overline{\psi}_{\xi m}] = 0\end{aligned} \tag{4.7}$$

$$\begin{aligned}\sum_{n=1}^{N_T} N_{n,\xi\xi}(\xi_i)\overline{\psi}_n + \frac{1}{\xi_i}\sum_{m=1}^{N_S} M_m(\xi_i)\overline{\psi}_{\xi m} = \\ -\frac{F^2 L_{ref}^2 c_{ref}}{\varepsilon\varepsilon_0 \eta RT}\{z_f \overline{c_f} + \sum_j^n \{z_j[\sum_{n=1}^{N_T} N_n(\xi_i)\overline{c_n^j} + \sum_{m=1}^{N_S}(\xi_i - \sum_{n=1}^{N_T} N_n(\xi_i)\xi_n)M_m(\xi_i)\overline{c_{\xi m}^j}]\}\}\end{aligned} \tag{4.8}$$

The corresponding auxiliary equations are obtained as

$$\sum_{n=1}^{N_T} N_{n,\xi}(\xi_i)\overline{c_n^j} - \sum_{m=1}^{N_S}(\sum_{n=1}^{N_T} N_{n,\xi}(\xi_i)\xi_n)M_m(\xi_i)\overline{c_{\xi m}^j} = 0, \tag{4.9}$$

$$\sum_{n=1}^{N_T} N_{n,\xi}(\xi_i)\overline{\psi}_n - \sum_{m=1}^{N_S}(\sum_{n=1}^{N_T} N_{n,\xi}(\xi_i)\xi_n)M_m(\xi_i)\overline{\psi}_{\xi m} = 0. \tag{4.10}$$

As described in the computational flow chart shown in Figure 2.3, after discretization of the Poisson-Nernst-Planck governing equations, the MECtherm

model, consisting of the transcendental equation (2.11) and nonlinear coupled Poisson-Nernst-Planck partial differential equations (2.21) and (2.22), will be solved by a hierarchical Newton iteration technique. In the inner iteration, the ionic concentrations c_j and electric potential ψ are computed simultaneously by the coupled equations (2.21) and (2.22). Then, substituting the coupled results into the outer iteration, the polymer-network volume fraction ϕ is obtained by the transcendental equation (2.11). Subsequently, the computed ϕ is substituted into the inner iteration again for the next iterative step until all the ionic concentrations c_j, electric potential ψ and polymer-network volume fraction ϕ converge to the required accuracy.

4.2 Experimental comparisons

For examination of the present MECtherm model, a numerical comparison is conducted with the experimentally measured swelling data found in a published literature, where Hirotsu et al. (1987) carried out the experiment of the temperature sensitive ionized poly(*N*-isopropylacrylamide) (PNIPA) hydrogels immersed in pure water subject to a changing temperature. The PNIPA hydrogel is a typical thermo-shrinking material, and it is well known due to its distinctive property of unique alteration between hydrophilicity and hydrophobicity upon external temperature stimulation. When surrounding temperature is lower than the corresponding lower critical solution temperature (LCST), the PNIPA hydrogel behaves hydrophilic characteristic alluring more water since the hydrogen bonds form a stable shell around the hydrophobic groups. With increasing the external temperature, the hydrophobic characteristic unveils to free the entrapped water molecules from the network as the

hydrogen bond interactions become weakened or destroyed. When the temperature reaches to or is higher than the LCST, the hydrophobic interactions become fully dominant and the hydrogel is thoroughly dehydrated. As the water releases, the polymer chains in the hydrogel collapse abruptly and the phase separation of the PNIPA hydrogel occurs, which is often termed the volume phase transition.

In the simulation of the ionized PNIPA hydrogels immersed in pure water, only the governing equation (2.12) is required and solved independently. For the simulation to compare with the experimental data, several parameters from the experiment of the ionized PNIPA hydrogels are taken as the input data of the simulations. They are the initial fixed-charge density $c_f^0 = 8\text{mM}$ with the corresponding valence $z_f = -1$ and the initial polymer volume fraction at the reference configuration $\phi_0 = 0.07$. In the presently simulated temperature region, obviously it is reasonable that the change of the water density is negligibly small, and then the effect of the change on the volume phase transition of PNIPA hydrogels is negligible. As such, one can take the water molar volume as the popularly specified constant $\nu = 18.0\text{cm}^3/\text{mol}$. In addition, the effective crosslink densities $\nu_e = 1.4\times10^{-5}\,\text{mol}/\text{cm}^3$ and $1.0\times10^{-5}\,\text{mol}/\text{cm}^3$ are taken for the hydrogels without and with the fixed charges, respectively. The polymer-network interaction parameter χ is calculated by equations (2.5) to (2.8) based on the given data (Hirotsu, 1987; Hino, 1998), in which $\delta s = -4.717\times10^{-23}\,\text{J/K}$, $\delta h = -1.246\times10^{-20}\,\text{J}$, $\zeta = 0.698\,\text{kcal/mol}$ and $\zeta_{12}/\zeta = -7$.

The comparison of the simulated results with the experimental data is shown in Figure 4.1 for the swelling equilibrium of the PNIPA hydrogels with and without fixed charges immersed in the pure water within the temperature range of 20-50°C. It

is observed from the figure that the simulated results agree well with the experimental data. It is also known that the fixed charges attached onto the polymer network enhance the swelling capability of ionized hydrogels, and also increase the lower critical solution temperature (LCST), as compared with the case of the hydrogels without fixed charges. At about temperature $T = 34.3°C$, the unionized PNIPA hydrogels undergo a continuous volume change, while the ionized PNIPA hydrogels exhibit a discontinuous volume phase transition at about temperature 35.6°C. The temperature of volume phase transition of the ionized PNIPA hydrogel is about 1°C higher than that of the unionized hydrogel. As the temperature increases, the volume swelling ratios of both the hydrogels decrease due to the shrinking properties. Furthermore, the swelling equilibrium curves of the hydrogels tend to be merged together at the temperature above 40.0°C, where the hydrogels are almost fully dehydrated.

4.3 Parameter Studies on swelling equilibrium

In this section, several parameter studies are carried out for analysis of swelling equilibrium behavior of the responsive PNIPA hydrogels with fixed charges immersed in univalent electrolyte solution, instead of pure water. The effects of several important physical parameters on volume phase transition of PNIPA hydrogels in swelling equilibrium state are discussed in details, including the initial fixed charge density c_f^0, bathing solution concentration c^*, effective crosslink density ν_e and initial polymer volume fraction ϕ_0.

4.3.1 Effect of initial fixed charge density

For discussion of the influence of the initial fixed charge density c_f^0 on the swell equilibrium of the PNIPA hydrogels, Figures 4.2 to 4.6 are plotted for the variation of the swelling ratio V/V_0 with the temperature and the distributions of the mobile ionic concentrations c_j, fixed charge density c_f, as well as electric potential ψ at different c_f^0 and T. In the view of theoretical analysis, when the thermo-sensitive ionized PNIPA hydrogels are immersed in the electrolyte bathing solution, the hydrogels will experience a dynamic process of volume change before the swelling equilibrium is finally achieved. After the hydrogels are placed into in the electrolyte solution, the negatively charged groups attached to the polymer chains are compensated by the cations diffusing into the hydrogel from the external solution, which results in the increase of the cation concentration within the hydrogel prior to the volume change. Here it is reasonably assumed that the ionic concentration in the external solution remains constant because of much more solution provided. The diffusion of the cations generates a concentration gradient between the hydrogel and the bathing solution, which is the source to generate the osmotic pressure to drive the dynamic swelling of hydrogel. The initial fixed charge density c_f^0 has significant influence on this process since a higher concentration increases the number of cations that need to diffuse into the hydrogels to compensate the ionized polymer chains, and enhance the magnitude of the concentration gradient. Thus, as initial fixed charge density c_f^0 increases, the concentration gradient increases. This will generate higher osmotic pressure, resulting in larger swelling of the hydrogels.

In order to investigate the influence of initial fixed charge density c_f^0 on the swelling equilibrium behavior, three thermo-sensitive ionized PNIPA hydrogels with

different initial fixed charge densities are simulated when they are immersed in univalent electrolyte solution, as shown in Figure 4.2, where the case corresponding to the initial fixed charge density c_f^0=1mM is represented by the dashed line, c_f^0=5mM by the solid line and c_f^0=10mM by the dotted line, and the univalent electrolyte bathing solution c^*=20mM. It can be seen from the figure that the computed LCST at the initial fixed charge density c_f^0=5mM is higher than that at c_f^0=1mM, and lower than that at c_f^0=10mM. Also, the temperature range of volume phase transition for the ionized hydrogels with higher fixed charge density is broader than that of the hydrogels with lower density.

To investigate the influences of the temperature T and the initial fixed charge density c_f^0 on the distributions of mobile ion concentrations c_j and fixed charge density c_f as well as electric potentials ψ in swelling equilibrium state. Figures 4.3 to 4.6 are presented for the cylindrical ionized PNIPA hydrogels with different initial fixed charge densities c_f^0=1mM, 5mM and 10mM, and the concentration of univalent electrolyte bathing solution c^*=20mM.

Figure 4.3(a) shows the concentration distributions of the mobile cation and anion in both the interior hydrogels and exterior bathing solution at temperature T=30°C, and Figure 4.4(a) shows those at temperature T=40°C. The distributions of fixed charge density c_f in the interior hydrogels and exterior bathing solution in swelling state are plotted in Figure 4.3(b) at temperature T=30°C and in Figure 4.4(b) at temperature T=40°C. Figures 4.3(a) and 4.4(a) predict that, for a given initial fixed charge density c_f^0, the mobile cation concentration within the PNIPA hydrogels at

temperature T=40°C is larger than that at T=30°C, but the opposite conclusion is drawn for the mobile anion concentration. Similarly, at a given temperature, the mobile cation concentration within the PNIPA hydrogels with larger initial fixed charge density is higher, while the opposite results are obtained for the mobile anion concentration. The higher the fixed charge density is, the larger the difference of mobile ion concentrations between interior and exterior hydrogel is. From Figures 4.3(a) and 4.3(b), it is seen that the total concentrations of all the mobile ions (cation and anion) and fixed charge are just compensated despite the individual concentration differences of the mobile ions and fixed charge density. Similar phenomena at T=40°C are also observed in Figures 4.4(a) and 4.4(b).

The distributions of the electric potentials of both the interior hydrogels and exterior bathing solution at temperature 30°C are plotted in Figure 4.5, and those at temperature 40°C in Figure 4.6. For a given initial fixed charge density c_f^0, the electric potential within the PNIPA hydrogels at temperature T=30°C is much higher than that at T=40°C. In the same manner, at a given temperature, the electric potential within the PNIPA hydrogels decreases with the increase of the initial fixed charge density c_f^0.

In addition, after comparison of the case at T=30°C with the corresponding case at T=40°C in Figures 4.3 to 4.6, it is noted that the hydrogel-solution interfaces move with the temperature. Thus they also demonstrate evidently that the polymer network volume fraction at temperature T=40°C is higher than that at T=30°C, due to the thermal shrinking characteristics of the ionized PNIPA hydrogels.

4.3.2 Effect of bathing solution concentration

For analysis of the influence of bathing solution concentration c^* on the response behavior of the PNIPA hydrogels in swelling equilibrium, Figures 4.7 to 4.11 are presented for the relationship between the swelling ratio V/V_0 and the temperature T, and the variation of the mobile ions and fixed charge as well as electric potential along the radial coordinates under different c^* and T. Theoretically, for a thermo-sensitive ionized PNIPA hydrogel immersed in pure water, the swelling equilibrium state is achieved when the total osmotic pressure is equal to zero. However, this equilibrium state can be simply destroyed by introducing the electrolyte into the pure water, and accordingly a dynamic volume change process will undergo until a new equilibrium is reached. At lower electrolyte concentration or the special case of pure water, the negative charges of the PNIPA hydrogel network are neutralized by counter hydrogen ions. As the electrolyte concentration increases, the hydrogen ions within the PNIPA hydrogel are replaced by the diffusive mobile cations from the bathing solution. If we further increase the electrolyte concentration in the system, more cations and anions would like to diffuse into the hydrogel from the external solution and then the overall concentration of mobile ions within the hydrogel is getting higher. However, the concentration difference between the interior hydrogel and exterior bathing solution is reduced, and consequently the driving force of swelling decreases gradually, which means that the swelling ratio becomes low.

For the present discussions, the thermo-sensitive ionized PNIPA hydrogels with invariable initial fixed charge density, c_f^0=5mM, are simulated for the effects of ionic concentration of bathing solution on swelling behavior. Figure 4.7 shows the variation of the swelling ratio V/V_0 of the hydrogels with temperature T subject to

different bathing solution concentrations c^*, namely pure water represented by a doted dash line, 5mM by a dotted line, 20mM by a solid line and 100mM by a dashed line, respectively. It is observed from the figure that simulating results verify the above theoretical analysis, in which the PNIPA hydrogels placed in pure water have the larger swelling ratio than those in electrolyte solution. With the increase of the ionic concentration of bathing solution, the swelling ratio decreases, and the temperature of volume phase transition also decreases. After the temperature increases above 40°C, they become completely dehydrated regardless of the ionic concentration of bathing solution.

In order to analyse the influences of the bathing solution concentration and temperature on the distributions of mobile ion concentrations, fixed charge density and electric potentials in swelling equilibrium, Figures 4.8 to 4.11 are generated for the ionized cylindrical PNIPA hydrogels immersed in different univalent electrolyte bathing solution.

Figure 4.8(a) shows the concentration distributions of the mobile cation and anion of the interior hydrogels and exterior bathing solution at temperature T=30°C, and Figure 4.9(a) shows those at temperature T=40°C. The distributions of fixed charge density in swelling equilibrium are plotted in Figure 4.8(b) at T=30°C and 4.9(b) at T=40°C, respectively. It is observed from Figures 4.8(a) and 4.9(a) that, for a given electrolyte bathing solution, the mobile cation concentration in the PNIPA hydrogels at temperature T=40°C is higher than that at T=30°C, but the opposite trend is for the mobile anion concentration. At a given temperature, with increasing the concentration c^* of bathing solution, the mobile cation concentration in the PNIPA hydrogels increases, while the mobile anion concentration decreases. As the

ionic concentration of bathing solution increases, the difference of mobile ion concentrations decreases between interior and exterior hydrogel. Figures 4.8 and 4.9 also demonstrate the phenomena where all the concentrations of mobile ions and fixed charge are compensated.

The distributions of the electric potentials of the interior hydrogels and the exterior bathing solution are shown in Figure 4.10 at T=30°C and Figure 4.11 at T=40°C, respectively. For a given electrolyte bathing solution, the electric potential within the PNIPA hydrogels at temperature T=30°C is much higher than that at T=40°C. Similarly, for a given temperature T, the electric potential within the PNIPA hydrogels increases with the increase of the ionic concentration of electrolyte bathing solution, which is different from the case in study on the effects of initial fixed charge c_f^0.

4.3.3 Effect of effective crosslink density

In order to study the influence of crosslink density, the relations between the temperature T and swelling ratio V/V_0 are illustrated in Figure 4.12, subjected to different crosslink densities ν_e. Distributions of the ionic concentrations, fixed charge density and electric potential with different ν_e and T are also illustrated in Figures 4.13 to 4.16. As well known, the crosslinking induces the formation of chemical bonds between linear polymer molecules, and it also leads to form infinite networks. The formed crosslinking divides a long chain into the connected short chains and thus forms numerous pores inside the hydrogels. Usually the hydrogels in state of large expansion contain a large amount of water in the pores. At swelling equilibrium state, the water uptake mostly depends on the crosslink density. As the crosslink density

increases, the network becomes stiffer, the pore size becomes smaller, and the water uptake decreases. Therefore, the increase of the crosslink density will reduce the porous volume within the hydrogel network structure, and provide smaller space for water uptake, which leads to a lower swelling ratio in equilibrium state.

In the present simulations for the effects of effective crosslink density ν_e on the swelling ratio V/V_0 in equilibrium state, three thermo-sensitive ionized PNIPA hydrogels are considered with different crosslink densities when immersed in univalent electrolyte bathing solution, in which the initial fixed charge density c_f^0=5mM, and the concentration of univalent electrolyte bathing solution $c^* = 20$mM. The hydrogel swelling ratio V/V_0 in equilibrium state versus temperature is shown in Figure 4.12, where hydrogel with the effective crosslink density ν_e=0.006mM is represented by dotted line, ν_e=0.01mM by solid line and ν_e=0.014mM by dashed line. It is seen from the figure that, regardless of crosslink densities, the swelling ratios V/V_0 of equilibrium thermo-sensitive PNIPA hydrogels have similar profiles as a function of temperature. Their LCSTs or the volume phase transition temperatures have nearly no shift for the hydrogels, in which all lie in the vicinity of 34.6°C. Figure 4.12 also shows that, at the temperature below LCST, the volume swelling ratio V/V_0 of the equilibrium PNIPA hydrogel with the effective crosslink density ν_e=0.010mM is larger than that with larger ν_e=0.014mM, and smaller than that with lower ν_e=0.006mM. The equilibrium volume changes of low crosslink density hydrogels are greater than those with high crosslink density at temperature below LCST.

To demonstrate the influence of the temperature T and effective crosslink density ν_e on the distributions of the mobile ion concentrations, fixed charge density

and electric potential along the radial coordinate in swelling equilibrium state, Figures 4.13 to 4.16 are generated for the ionized cylindrical PNIPA hydrogels immersed in the univalent electrolyte bathing solution.

Concentration distributions of the mobile cation and anion in both the interior hydrogels and exterior bathing solution are shown in Figure 4.13(a) at temperature T=30°C and Figure 4.14(a) at temperature T=40°C. Correspondingly, the distributions of fixed charge density c_f in equilibrium state are plotted in Figure 4.13(b) at T=30°C and Figure 4.14(b) at T=40°C. Figures 4.13(a) and 4.14(a) show that, for a given effective crosslink density ν_e, the mobile cation concentration in the interior PNIPA hydrogels at temperature T=40°C is higher than that at T=30°C, which is caused by depleting water from the hydrogels due to the collapse. At temperature T=30°C, the mobile cation concentration in the interior PNIPA hydrogels is higher with increasing the effective crosslink density ν_e. The opposite trends are observed for the mobile anion concentration. As the effective crosslink density ν_e increases, the mobile anion concentration decreases. Additionally, the increase of the effective crosslink density ν_e makes the larger difference of ionic concentrations between interior hydrogel and exterior solution. At temperature T=40°C, all mobile ion concentrations in both the hydrogels and solution are equal to each other for different crosslink densities ν_e because of the same swelling ratio, as portrayed in Figure 4.12. Figures 4.13 and 4.14 demonstrate similar phenomena to those in Figures 4.3, where all the concentrations of mobile cation and anion, and fixed charge are compensated.

Distributions of the electric potential in both the interior hydrogels and exterior bathing solution are plotted in Figure 4.15 at temperature T=30°C and in Figure 4.16 at temperature T=40°C. For a given effective crosslink density ν_e, the electric potential in the PNIPA hydrogel at temperature T=30°C is much higher than that at T=40°C. At the temperature T below the volume phase transition temperature such as T=30°C, the electric potential in the PNIPA hydrogels decreases with increasing the effective crosslink density ν_e. At the temperature above the volume phase transition temperature such as T=40°C, the electrical potentials under different effective crosslink densities ν_e are equal in both the hydrogels and solution because of the same swelling ratio V/V_0.

4.3.4 Effect of initial polymer volume fraction

Initial polymer volume fraction ϕ_0 is defined at the reference state by the product of the molar volume and concentration of the monomeric unit at the preparation of hydrogels. Crosslinking agent induces the connection of these monomeric units to form networks. Initially a hydrogel is in the dry state, solvent has to diffuse into the networks to fulfill the free-volume, which is not occupied by the polymer chains in the hydrogels. Influence of the initial polymer volume fraction ϕ_0 at a constant crosslink density is different from that of the effective crosslink density in the hydrogels.

In order to examine the effects of initial polymer volume fraction ϕ_0 on the volume swelling ratio V/V_0 in equilibrium state, three thermo-sensitive ionized PNIPA hydrogels with different initial polymer volume fractions ϕ_0 are simulated

when immersed in univalent electrolyte solution, where the initial fixed charge density c_f^0=5mM, and the univalent electrolyte bathing solution $c^* = 20$mM. Figure 4.17 shows the response behavior of the hydrogels with different initial polymer volume fractions, ϕ_0=0.05 represented by dotted line, ϕ_0=0.07 by solid line and ϕ_0=0.09 by dashed line. It is seen from the figure that the profiles of volume swelling ratio V/V_0 of equilibrium thermo-sensitive PNIPA hydrogels are quite different for different initial polymer volume fractions. At the temperature below LCST, the volume swelling ratio V/V_0 of the equilibrium PNIPA hydrogel with ϕ_0=0.07 is larger than that with smaller ϕ_0=0.05, and is smaller than that with bigger ϕ_0=0.09. In the contrast, the computed LCST for the initial polymer volume fraction ϕ_0=0.07 is greater than that for ϕ_0=0.09, and is lower than that for ϕ_0=0.05, namely, the computed LCST decreases with increasing the initial polymer volume fraction ϕ_0. Obviously, the volume change of equilibrium hydrogel with larger initial polymer volume fraction ϕ_0 is greater than that with smaller ϕ_0 at the temperatures below LCST. At temperature above LCST, the volume swelling ratio for the equilibrium hydrogels with larger initial polymer volume fraction ϕ_0 is smaller than that with lower ϕ_0.

For analysis of the influence of the temperature T and initial polymer volume fraction ϕ_0 on the distributions of mobile ion concentrations, fixed charge density and electric potential in swelling equilibrium state, Figures 4.18 to 4.21 are plotted for the ionized cylindrical PNIPA hydrogels immersed in the univalent electrolyte bathing solution.

The concentration distributions of the mobile cation and anion in both the interior hydrogels and exterior bathing solution are demonstrated in Figure 4.18(a) at temperature T=30°C and Figure 4.19(a) at temperature T=40°C. Distributions of fixed charge density in swelling state are plotted in Figure 4.18(b) at T=30°C and Figure 4.19(b) at T=40°C. Figures 4.18(a) and 4.19(a) show that, for a given initial polymer volume fraction ϕ_0, the mobile cation concentration in the interior PNIPA hydrogels at temperature T=40°C is higher than that at T=30°C. At a given temperature T, the mobile cation concentration in the interior PNIPA hydrogels is higher for smaller initial polymer volume fraction ϕ_0. The opposite trends are observed for the mobile anion concentration, namely as the initial polymer volume fraction ϕ_0 increases, the mobile anion concentration increases, and the difference of mobile ion concentrations decrease between interior hydrogel and exterior bathing solution.

Distributions of the electric potential in both the interior hydrogels and exterior bathing solution are plotted in Figure 4.20 at temperature T=30°C and in Figure 4.21 at temperature T=40°C. For a given initial polymer volume fraction ϕ_0, the electric potential in the interior PNIPA hydrogel at temperature T=30°C is much higher than that at T=40°C. At a given temperature, the electric potential in the interior PNIPA hydrogels increases accordingly with increasing the initial polymer volume fraction ϕ_0.

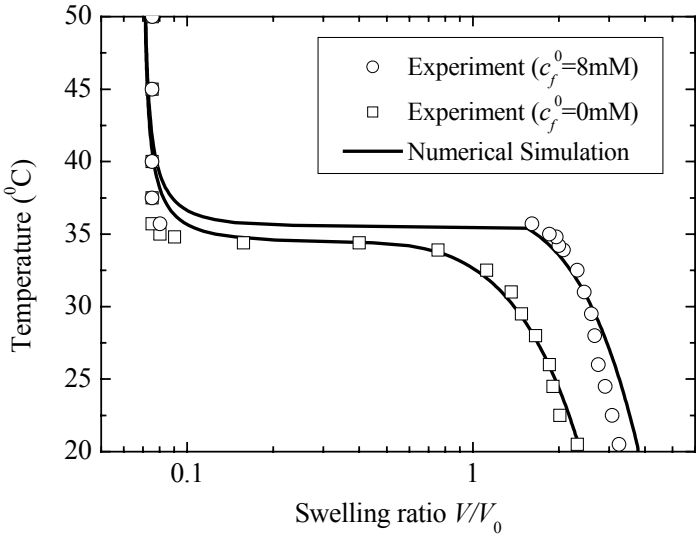

Figure 4.1 Comparison of numerical simulations with the experimental swelling data for temperature-sensitive PNIPA hydrogels in pure water.

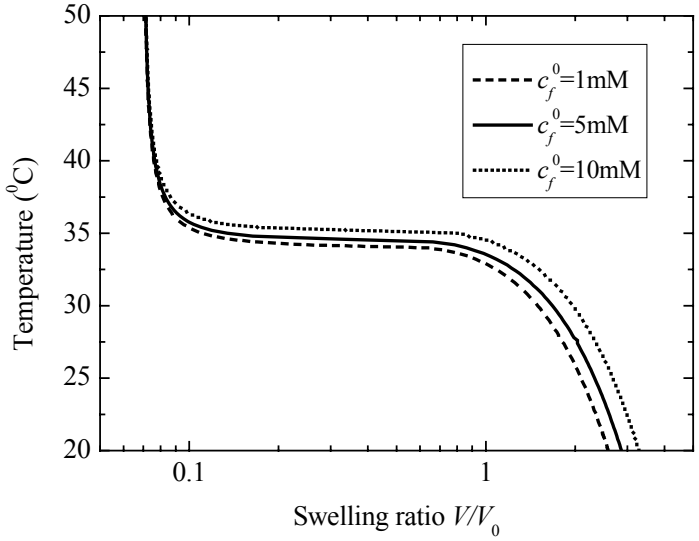

Figure 4.2 Relation between the temperature and swelling ratio V/V_0 of equilibrium volume for the ionized hydrogels with different initial fixed charge densities c_f^0 immersed in the univalent electrolyte solution $c^* = 20\,\text{mM}$.

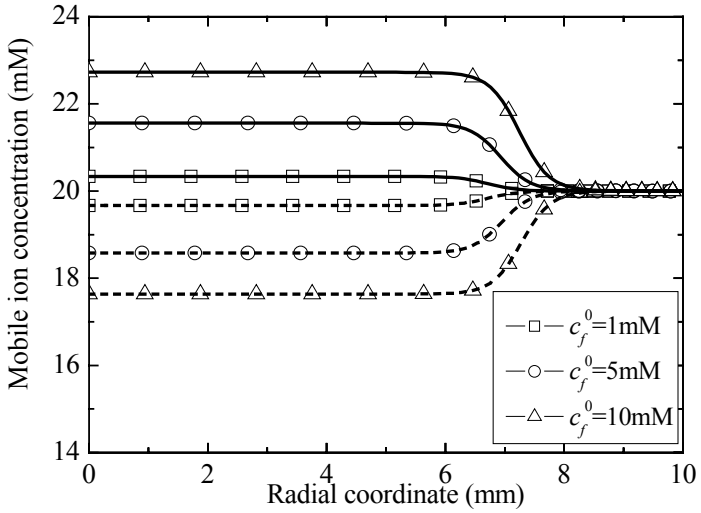

(a)

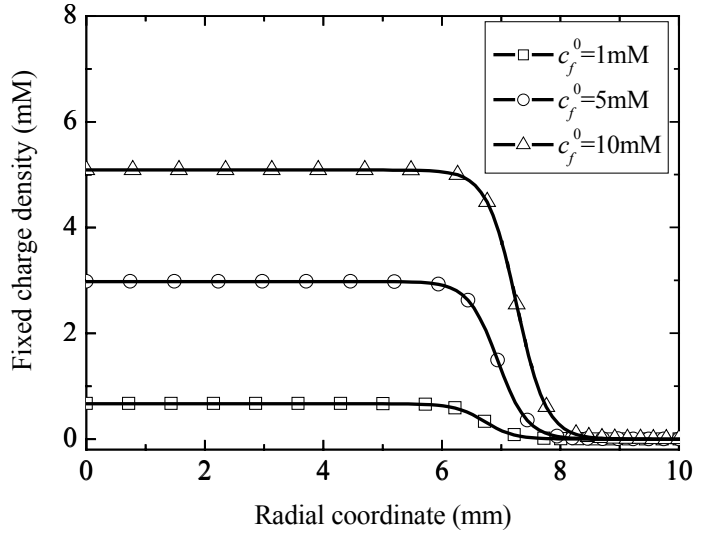

(b)

Figure 4.3 Distributions of the mobile cation (solid line) and anion (dash line) concentrations (a), and the fixed charge densities (b) versus radial coordinate for the ionized hydrogels with different initial fixed charge densities c_f^0 at temperature T =30°C prior to volume phase transition.

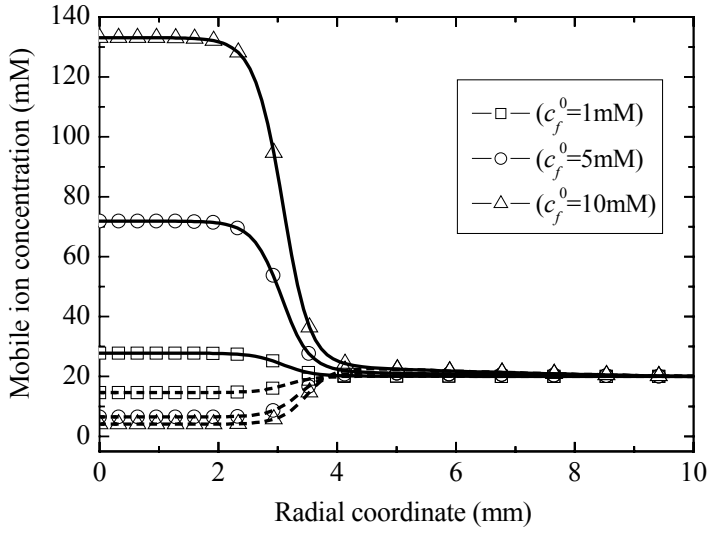

(a)

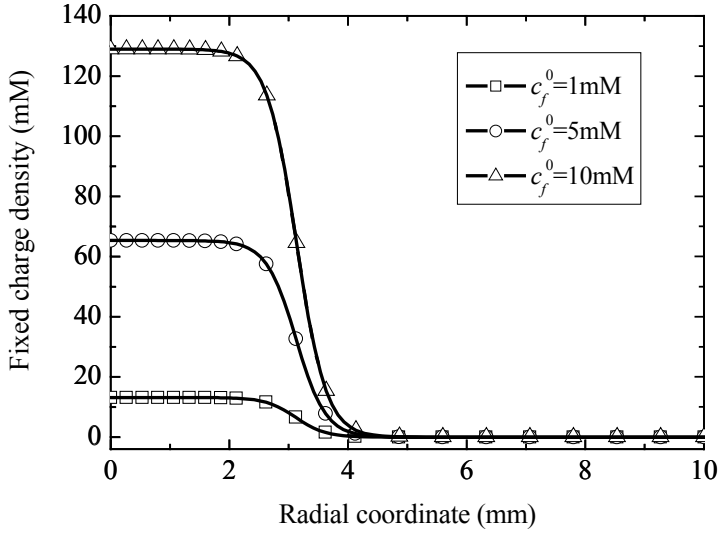

(b)

Figure 4.4 Distributions of the mobile cation (solid line) and anion (dash line) concentrations (a), and the fixed charge densities (b) versus radial coordinate for the ionized hydrogels with different initial fixed charge densities c_f^0 at temperature T=40°C posterior to volume phase transition.

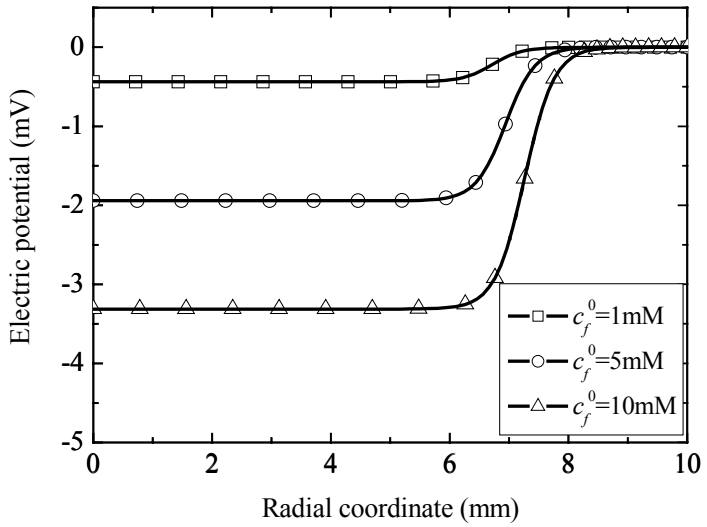

Figure 4.5 Distributions of electric potentials versus radial coordinate for the ionized hydrogels with different initial fixed charge densities c_f^0 at temperature T=30°C prior to volume phase transition.

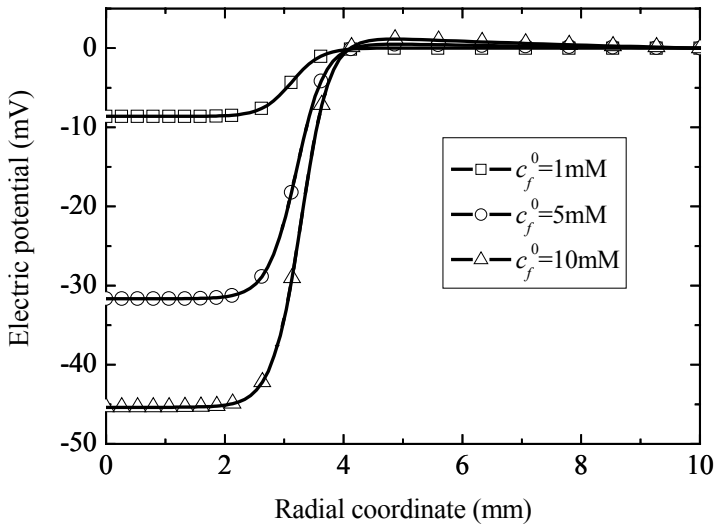

Figure 4.6 Distributions of electric potentials versus radial coordinate for the ionized hydrogels with different initial fixed charge densities c_f^0 at temperature T=40°C posterior to volume phase transition.

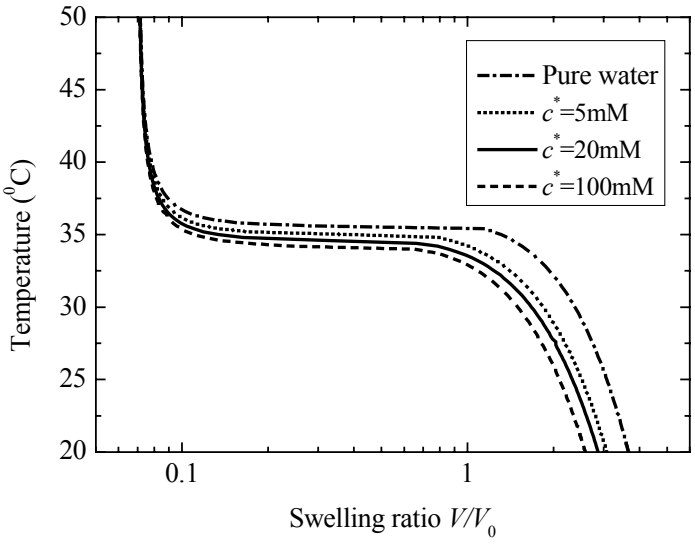

Figure 4.7 Relation between the temperature and swelling ratio V/V_0 of equilibrium volume for the ionized PNIPA hydrogels with initial fixed charge density c_f^0=5mM immersed in pure water and different bathing solution concentrations c^*=5, 20 and 100mM, respectively.

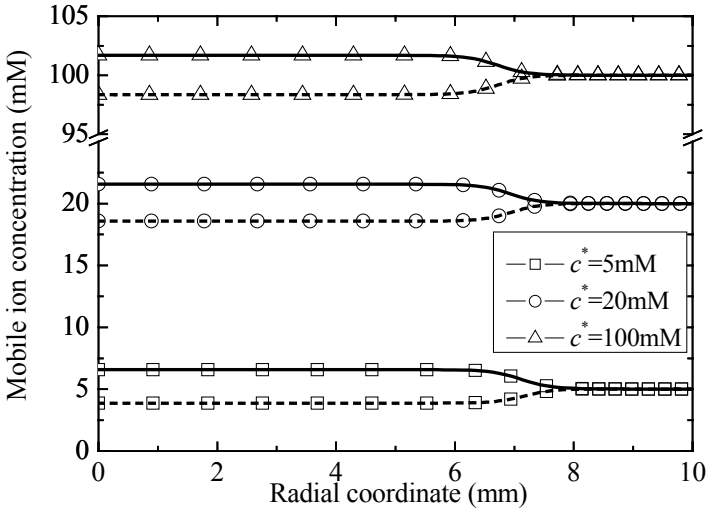

(a)

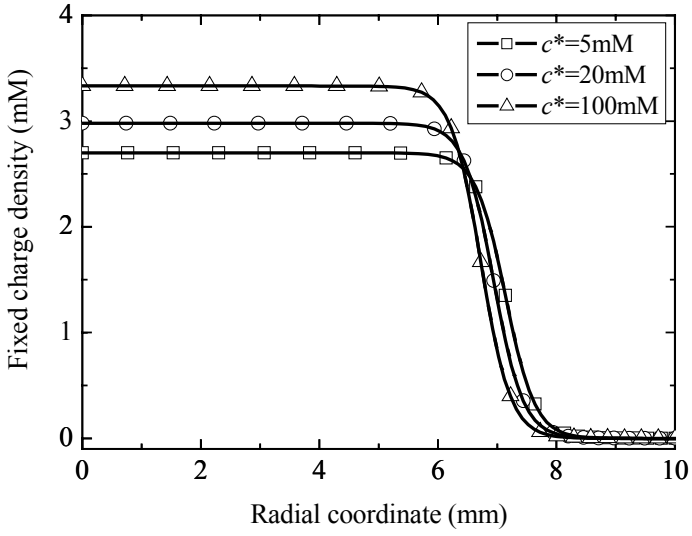

(b)

Figure 4.8 Distributions of the mobile cation (solid line) and anion (dash line) concentrations (a) , and the fixed charge densities (b) versus radial coordinate for the ionized PNIPA hydrogels with initial fixed charge density $c_f^0 = 5\,\mathrm{mM}$ immersed in different bathing solution concentrations c^* at temperature T=30°C.

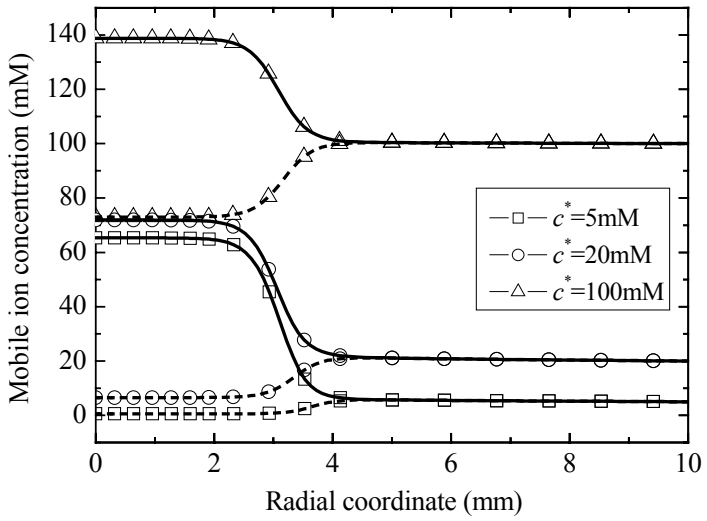

(a)

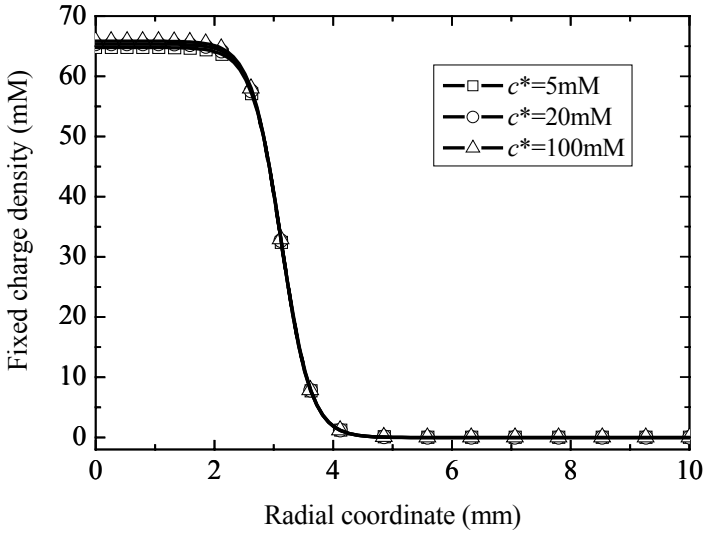

(b)

Figure 4.9 Distributions of the mobile cation (solid line) and anion (dash line) concentrations and the fixed charge densities (b) versus radial coordinate for the ionized PNIPA hydrogels with initial fixed charge density $c_f^0 = 5\,\mathrm{mM}$ immersed in different bathing solution concentrations c^* at temperature T=40°C.

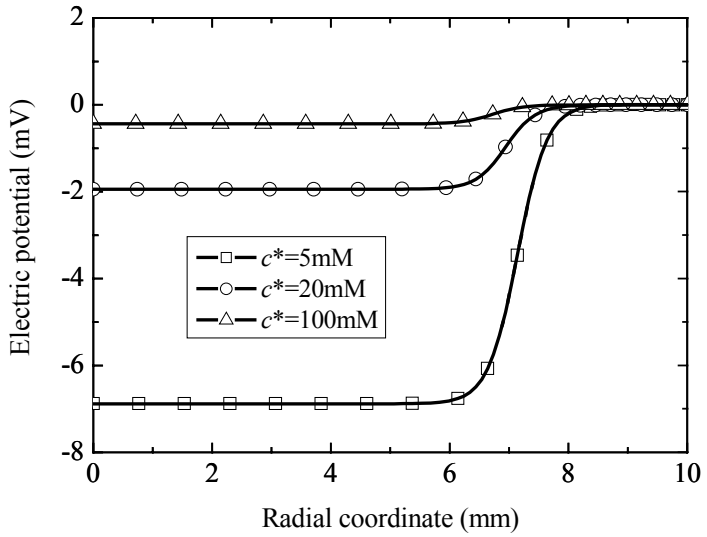

Figure 4.10 Distributions of electric potentials versus radial coordinate for the ionized PNIPA hydrogels with initial fixed charge density $c_f^0 = 5\,\mathrm{mM}$ immersed in different bathing solution concentrations c^* at temperature T=30°C.

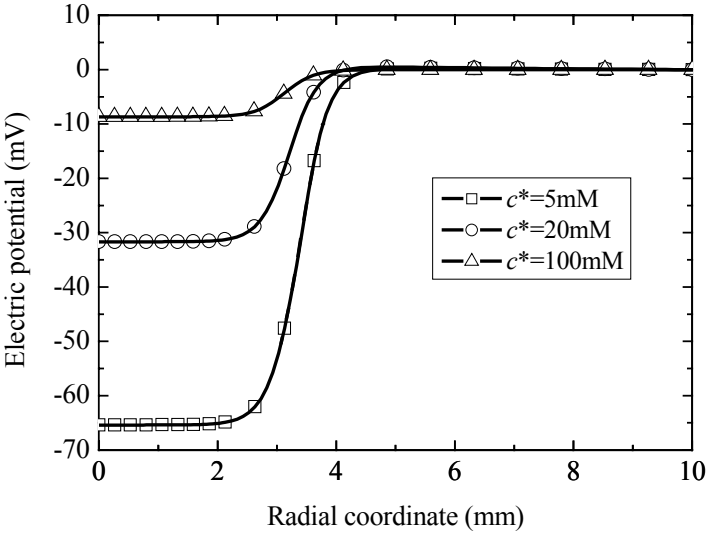

Figure 4.11 Distributions of electric potentials versus radial coordinate for the ionized PNIPA hydrogels with initial fixed charge density $c_f^0 = 5\,\mathrm{mM}$ immersed in different bathing solution concentrations c^* at temperature T=40°C.

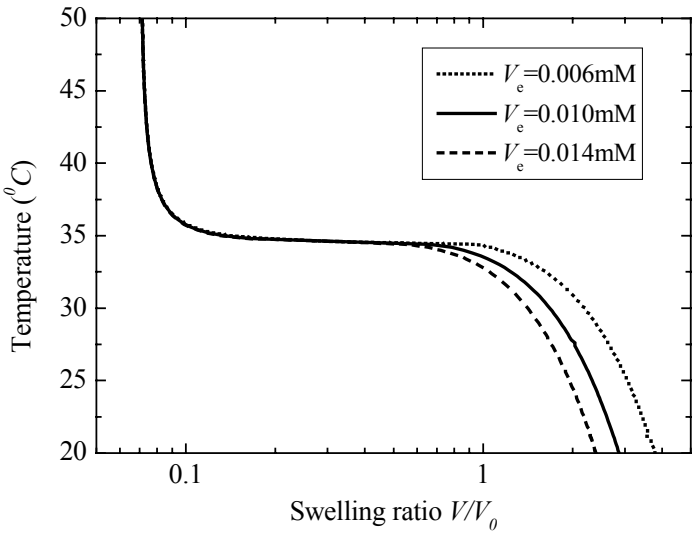

Figure 4.12 Relation between the temperature and swelling ratio V/V_0 of equilibrium volume for the ionized hydrogels with initial fixed charge density $c_f^0 = 5\,\mathrm{mM}$ and different crosslink densities ν_e immersed in the univalent electrolyte solution $c^* = 20\mathrm{mM}$.

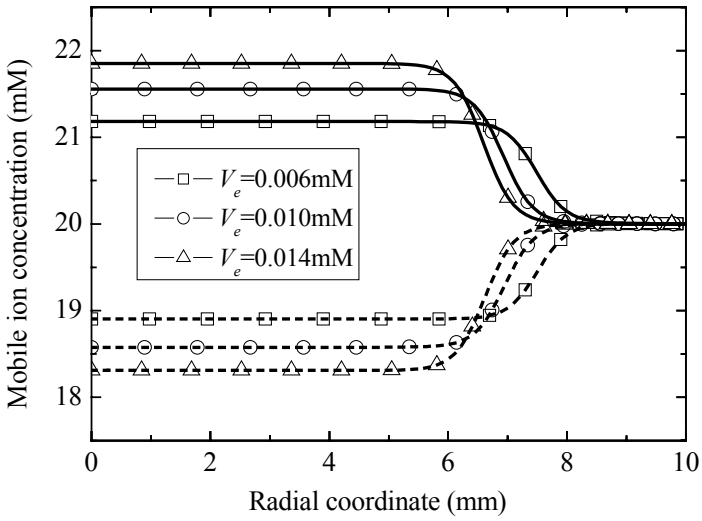

(a)

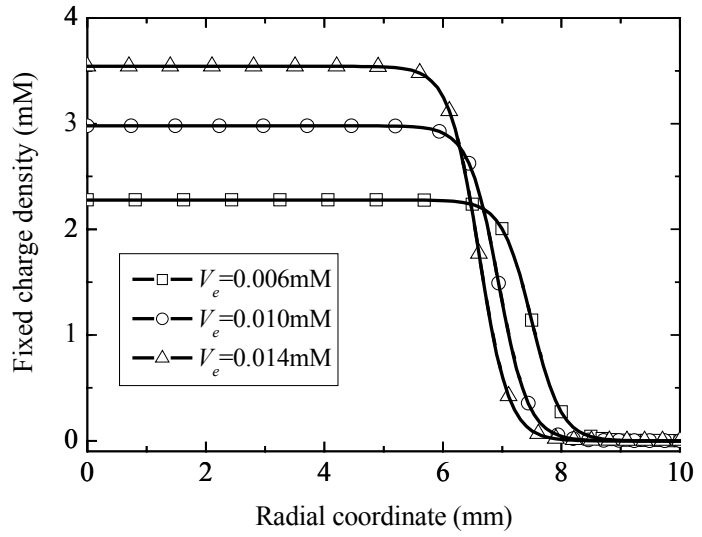

(b)

Figure 4.13 Distributions of the mobile cation (solid line) and anion (dash line) concentrations (a) and the fixed charge densities (b) versus radial coordinate for the ionized PNIPA hydrogels with initial fixed charge density $c_f^0 = 5\,\mathrm{mM}$ and different crosslink densities ν_e immersed in the univalent electrolyte solution $c^* = 20\mathrm{mM}$ at temperature T=30°C.

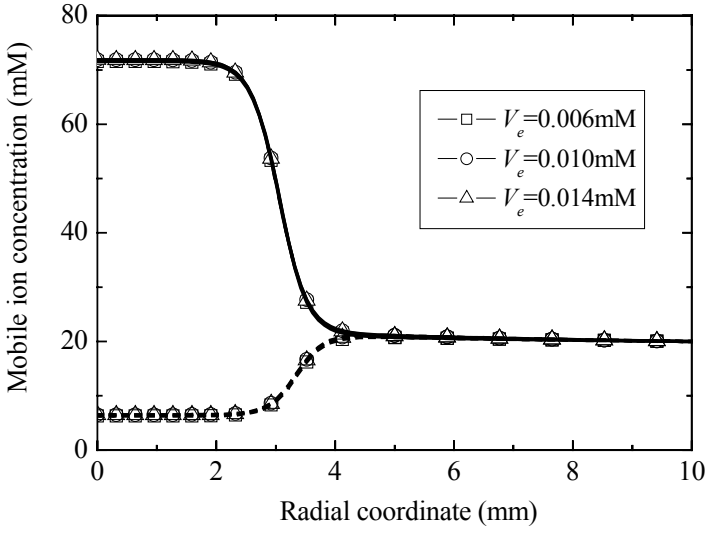

(a)

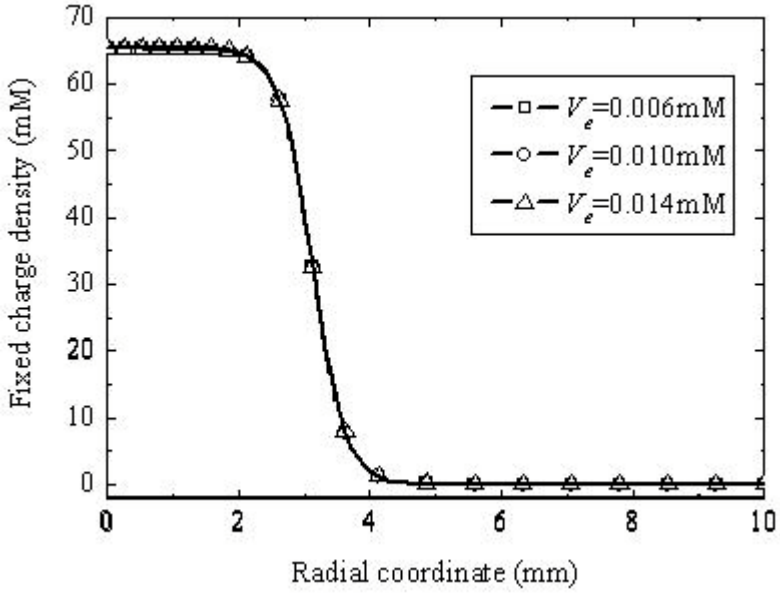

(b)

Figure 4.14 Distributions of the mobile cation (solid line) and anion (dash line) concentrations (a), and the fixed charge densities (b) versus radial coordinate for the ionized PNIPA hydrogels with initial fixed charge density $c_f^0 = 5\,\text{mM}$ and different crosslink densities ν_e immersed in the univalent electrolyte solution $c^* = 20\text{mM}$ at temperature T=40°C.

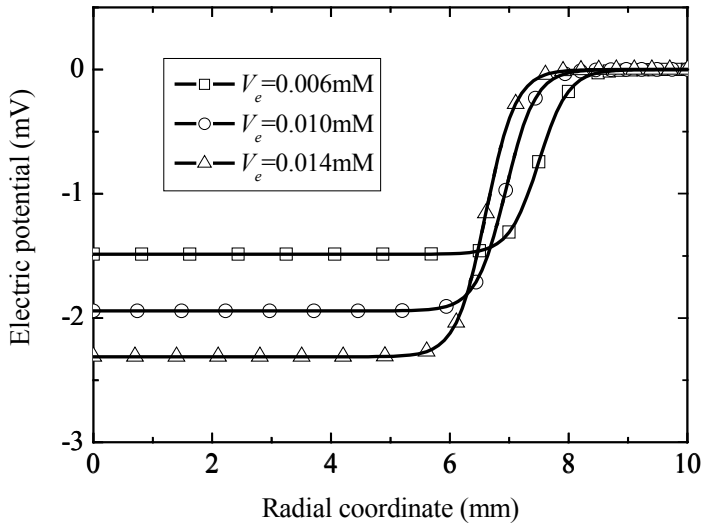

Figure 4.15 Distributions of electric potentials versus radial coordinate for the ionized PNIPA hydrogels with initial fixed charge density $c_f^0 = 5\,\text{mM}$ and different crosslink densities ν_e immersed in the univalent electrolyte solutions $c^* = 20\text{mM}$ at temperature T=30°C.

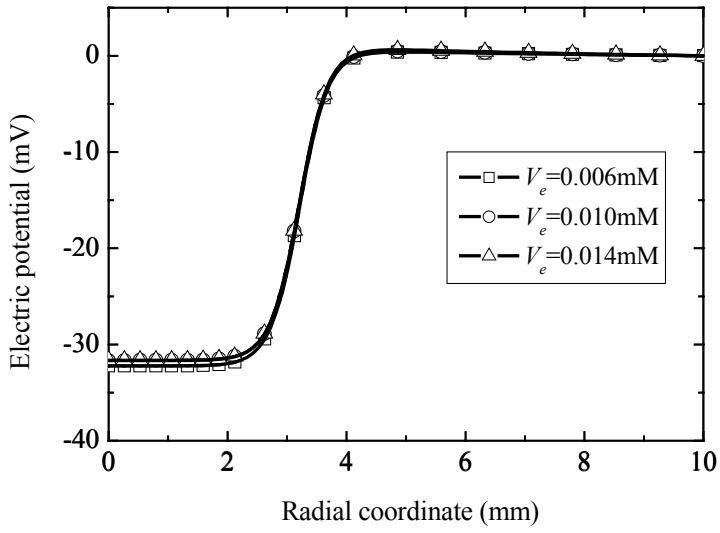

Figure 4.16 Distributions of electric potentials versus radial coordinate for the ionized PNIPA hydrogels with initial fixed charge density $c_f^0 = 5\,\text{mM}$ and different crosslink densities ν_e immersed in the univalent electrolyte solution $c^* = 20\text{mM}$ at temperature T=40°C.

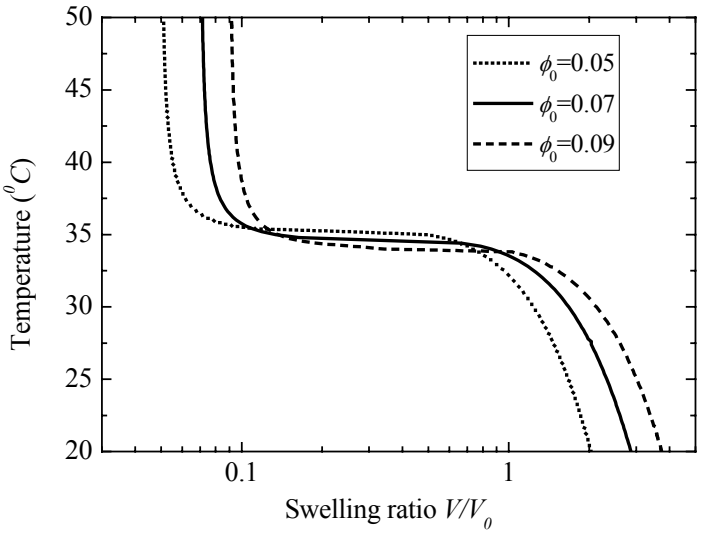

Figure 4.17 Relation between the temperature and swelling ratio V/V_0 of equilibrium volume for the ionized hydrogels with initial fixed charge density $c_f^0 = 5\text{mM}$ and different initial polymer volume fractions ϕ_0 immersed in the univalent electrolyte solution $c^* = 20\text{mM}$.

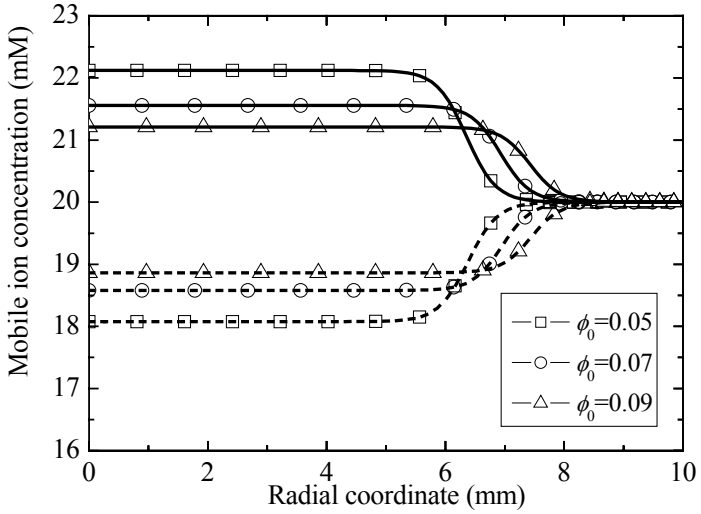

(a)

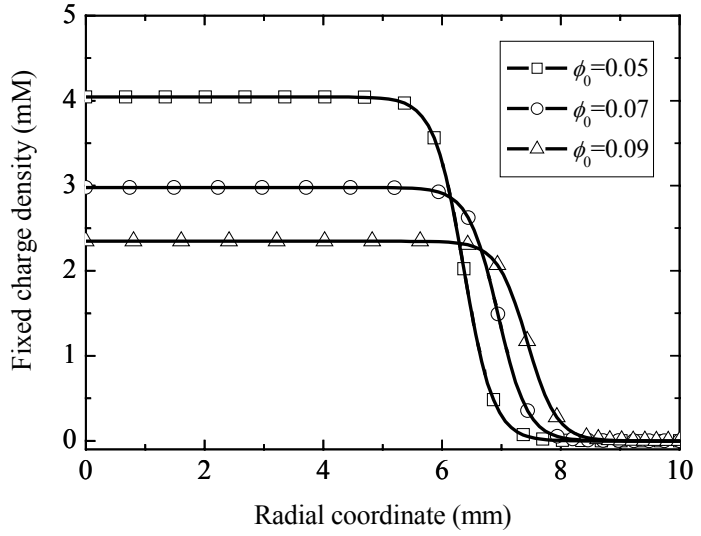

(b)

Figure 4.18 Distributions of the mobile cation (solid line) and anion (dash line) concentrations (a) and the fixed charge densities (b) versus radial coordinate for the ionized PNIPA hydrogels with initial fixed charge density $c_f^0 = 5\,\mathrm{mM}$ and different initial polymer volume fractions ϕ_0 immersed in the univalent electrolyte solution $c^* = 20\mathrm{mM}$ at temperature T=30°C.

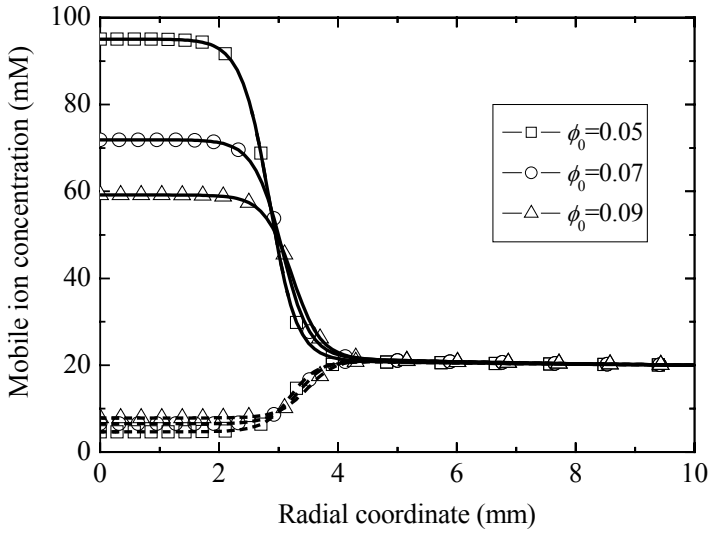

(a)

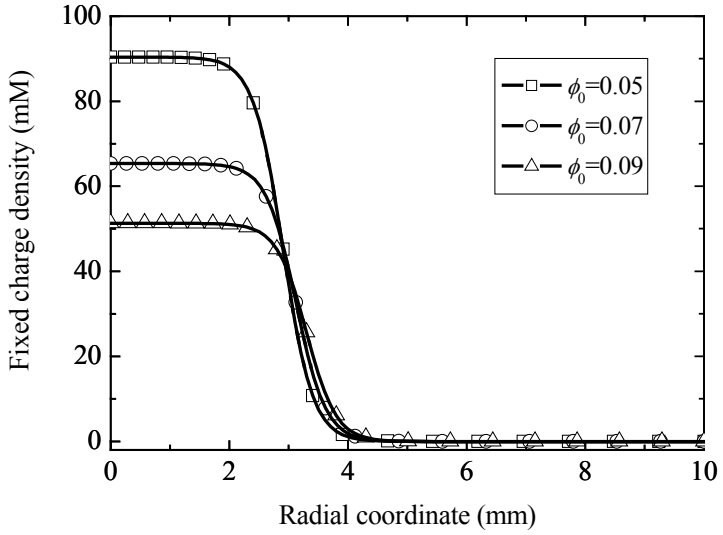

(b)

Figure 4.19 Distributions of the mobile cation (solid line) and anion (dash line) concentrations (a) and the fixed charge densities (b) versus radial coordinate for the ionized PNIPA hydrogels with initial fixed charge density $c_f^0 = 5\,\mathrm{mM}$ and different initial polymer volume fractions ϕ_0 immersed in the univalent electrolyte solution $c^* = 20\mathrm{mM}$ at temperature T =40°C.

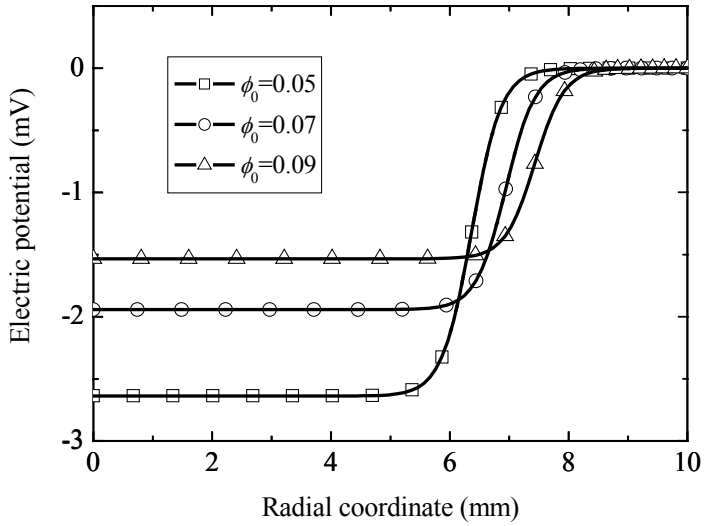

Figure 4.20 Distributions of electric potentials versus radial coordinate for the ionized PNIPA hydrogels with initial fixed charge density $c_f^0 = 5\,\text{mM}$ and different initial polymer volume fractions ϕ_0 immersed in the univalent electrolyte solution $c^* = 20\text{mM}$ at temperature T=30°C.

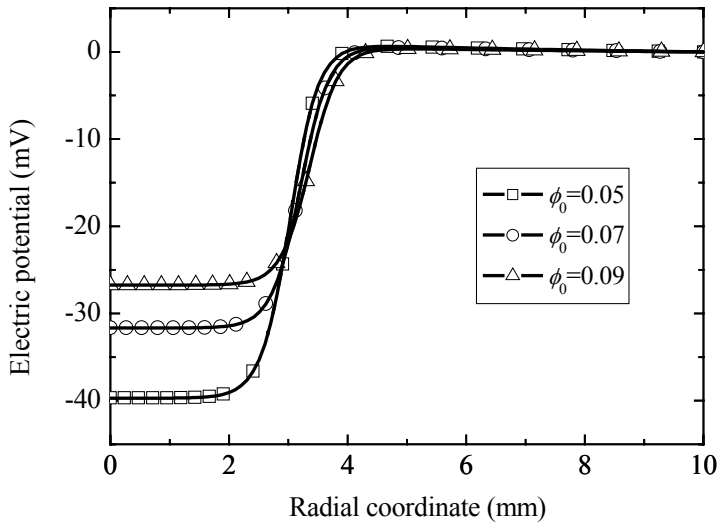

Figure 4.21 Distributions of electric potentials versus radial coordinate for the ionized PNIPA hydrogels with initial fixed charge density $c_f^0 = 5\,\text{mM}$ and different initial polymer volume fractions ϕ_0 immersed in the univalent electrolyte solution $c^* = 20\text{mM}$ at temperature T=40°C.

Chapter 5

Transient Model Development for Simulation of Drug Delivery from Microgels

In this chapter, a transient model is provided for simulation of drug delivery from microgels, where the controlled nifedipine release from the spherical chitosan microgels is investigated numerically. The mathematical model takes into account both drug dissolution and drug diffusion through the continuous matrices of spherical microgels. The effects of several important physical parameters on drug release are evaluated, including the microsphere radius, equivalent drug saturation concentration, drug diffusion coefficient, and drug dissolution rate constant.

5.1 Formulation of mathematical model

Nifedipine is a poorly water-soluble drug with solubility less than 10 mg/L (Liu et al., 2000). As a well-known calcium channel blocker, nifedipine is most commonly used for the treatment of hypertension, a chronic disease that affects 10~20% of the world population and induces cardiovascular complications (Hombreiro et al., 2003). However, many serious adverse effects associated with immediate nifedipine release have been revealed, such as hypotension, myocardial ischemia or infarction, ventricular fibrillation, and cerebral ischemia (Mansoor et al., 2002). Given the seriousness of the reported adverse events and the lack of any clinical documentation attesting to a benefit, Food and Drug Administration (FDA) of USA concluded that the use of immediately released nifedipine for hypertensive

emergencies is neither safe nor effective and therefore it should not be used (Grossman et al., 1996).

Microspheric drug release system has attracted increasing attention recently. Controlled nifedipine release was investigated experimentally by using various polymer-based microgels, such as spherical chitosan microgels, Eudragit microcapsules, and poly(DL lactide-co-glycolide acid) microspheres. However, no effort is made to develop mathematical model for simulation of the nifedipine release process due to the complexity. The objective of the present work is to present a model with consideration of dissolution and diffusion mechanisms for numerical investigation of the nifedipine release from chitosan microgels.

In general, the initial drug loading concentration C_0 in spherical microgels is greater than the drug saturation concentration C_s. This can be achieved either by preparation of a solution and total evaporation of the solvent, or by partial evaporation or phase inversion (Harland et al., 1988). When the polymeric microgels are put into a well stirred release medium, the following four mass transfer steps take place consequently (Hombreiro et al., 2003): (1) drug dissolution within the microgels; (2) drug diffusion within the matrices of microgels; (3) drug diffusion through the unstirred liquid boundary layers on the surfaces of the microgels; and (4) drug diffusion and convection within the release medium. Since the convective transport within the medium is usually fast compared with that of the diffusive mass, the convective transport can be neglected when calculating the overall rate of drug release from the polymeric microgels. Therefore, it is reasonable to assume that drug dissolution and diffusion from the continuous matrices of spherical microgels control the drug release in a well-stirred release medium.

The kinetics of drug release from the microgels with radius R can be simulated mathematically by the following partial differential governing equation (Harland et al., 1988),

$$\frac{\partial C(r,t)}{\partial t} = D(\frac{\partial^2 C(r,t)}{\partial r^2} + \frac{2}{r}\frac{\partial C(r,t)}{\partial r}) + k(\varepsilon C_s - C(r,t)), \tag{5.1}$$

and the following initial and boundary conditions for the drug release process in a well stirred release medium,

$$t = 0 \qquad 0 < r < R \qquad C(r,t) = \varepsilon C_s, \tag{5.2-a}$$

$$t > 0 \qquad r = 0 \qquad \frac{\partial C(r,t)}{\partial r} = 0, \tag{5.2-b}$$

$$t > 0 \qquad r = R \qquad C(r,t) = 0, \tag{5.2-c}$$

where $C(r,t)$ (g/cm^3) is the drug concentration at the radial position r (cm) of the microgel system at the release time t (s), D (cm^2/s) is the drug diffusion coefficient, k (s^{-1}) is the first-order drug dissolution rate constant, ε is a parameter for the polymeric network meshes of microgels and it is directly related to the cross-linking density of the polymeric microspheres. If C_s (g/cm^3) is defined as drug saturation concentration in the system, εC_s (g/cm^3) refers to the equivalent drug saturation concentration in microgels with a network mesh parameter ε.

The first term of the right-hand side in equation (5.1) is the well-known Fick's second law of diffusion for a spherical system (Crank, 1975), which describes the diffusion drug release process in the microgels due to the continuous dissolution of the drug. The second term of the right-hand side in equation (5.1) corresponds to the potential rate-limiting drug dissolution process (Harland et al., 1988). It is observed that, when the drug loading concentration C_0 is smaller than the drug saturation

concentration C_s, the equation (5.1) is reduced to the classic Fick's diffusion equation. Although the drug diffusion coefficient D in the polymeric microgels may be solvent-concentration dependent, usually it is reasonable to assume approximately a constant D for simplicity.

It is also assumed that the drug is uniformly distributed throughout the microgels with equivalent drug saturation concentration εC_s initially. Under perfect sink conditions, the release medium can be considered to be well stirred, thus the drug concentration outside of microgels is further assumed to be constant and equal to zero.

By defining dimensionless parameters (Harland et al., 1988), $\xi = r/R$ for dimensionless radius, $\tau = Dt/R^2$ for dimensionless Fourier time, $\beta = kR^2/D$ called dimensionless dissolution/diffusion number, and dimensionless concentration $\overline{C}(\xi,\tau) = 1 - C(r,t)/\varepsilon C_s$, which indicates the non-dimensional drug concentration additionally required to reach saturation dissolution, the partial differential governing equation (5.1) and initial and boundary conditions (5.2) are thus rewritten in the dimensionless forms as,

$$\frac{\partial \overline{C}(\xi,\tau)}{\partial \tau} = \frac{\partial^2 \overline{C}(\xi,\tau)}{\partial \xi^2} + \frac{2}{\xi}\frac{\partial \overline{C}(\xi,\tau)}{\partial \xi} - \beta \overline{C}(\xi,\tau), \tag{5.3}$$

$$\tau = 0 \qquad 0 < \xi < 1 \qquad \overline{C}(\xi,\tau) = 0 \qquad , \tag{5.4}$$

$$\tau > 0 \qquad \frac{\partial \overline{C}(\xi,\tau)}{\partial \xi} = 0 \text{ at } \xi = 0, \qquad \text{and} \qquad \overline{C}(\xi,\tau) = 1 \text{ at } \xi = 1. \tag{5.5}$$

After solving the set of above governing equation and conditions, $\overline{C}(\xi,\tau)$ is obtained and then the drug concentration $C(r,t)$ is computed. According to Fick's first law (Robert, 1996), the flux $J = J(r,t)$, the rate of drug transfer per unit area of section, is considered as,

$$J(r,t) = -D\frac{\partial C(r,t)}{\partial r}. \tag{5.6}$$

The rate of drug release from the microgels is thus calculated by (Robert, 1996)

$$\frac{\partial M_t}{\partial t} = AJ(r,t)\big|_{r=R}, \tag{5.7}$$

where A is the area of microgels with radius R, M_t represents the amount of drug released after time t and it can be calculated by integrating equation (5.7),

$$M_t = \int_0^t AJ(r,\bar{t})\big|_{r=R} d\bar{t} = 4\pi R^2 \int_0^t (-D\frac{\partial C(r,\bar{t})}{\partial r}\big|_{r=R}) d\bar{t} = -4\pi R^2 D\int_0^t \frac{\partial C(r,\bar{t})}{\partial r}\big|_{r=R} d\bar{t}. \tag{5.8}$$

5.2 Model implementations

To simulate the kinetics of drug release, the non-dimensional partial differential governing equation (5.3) at time τ is discretized in spatial domain by the Hermite-cloud method and discretized in time domain by linear interpolation technique as

$$\frac{\partial \overline{C}(\xi,\tau)}{\partial \tau} = \frac{\partial^2 \overline{C}(\xi,\tau)}{\partial \xi^2} + \frac{2}{\xi}\frac{\partial \overline{C}(\xi,\tau)}{\partial \xi} - \beta \overline{C}(\xi,\tau). \tag{5.9}$$

Using Hermite-cloud method for spatial discretization, we have,

$$\overline{C}(\xi,\tau) = \sum_{n=1}^{N_T} N_n(\xi)\overline{C}_n(\tau) + \sum_{m=1}^{N_S}(\xi - \sum_{n=1}^{N_T} N_n(\xi)\xi_n)M_m(\xi)\overline{C}_{\xi m}(\tau), \tag{5.10}$$

$$\overline{C}_\xi(\xi,\tau) = \frac{\partial \overline{C}(\xi,\tau)}{\partial \xi} = \sum_{m=1}^{N_S} M_m(\xi)\overline{C}_{\xi m}(\tau), \tag{5.11}$$

$$\frac{\partial^2 \overline{C}(\xi,\tau)}{\partial \xi^2} = \sum_{n=1}^{N_T} N_{n,\xi\xi}(\xi)\overline{C}_n(\tau). \tag{5.12}$$

Substituting equations (5.10) to (5.12) into equation (5.9), the drug release governing equation is discretized at ξ_i of spatial domain in the following form,

$$\begin{aligned}\frac{\partial \overline{C}(\xi_i,\tau)}{\partial \tau} &= \sum_{n=1}^{N_T}(N_{n,\xi\xi}(\xi_i)-\beta N_n(\xi_i))\overline{C}_n(\tau) \\ &+(\frac{2}{\xi_i}-\beta(\xi_i-\sum_{n=1}^{N_T}N_n(\xi_i)\xi_n))\sum_{m=1}^{N_S}M_m(\xi_i)\overline{C}_{\xi m}(\tau)\end{aligned}. \tag{5.13}$$

By the linear interpolation technique, a weighted average of the time derivative $\partial\overline{C}/\partial\tau$ can be approximated at two consecutive time steps as follows (Reddy, 1993),

$$(1-\lambda)\frac{\partial \overline{C}(\xi_i,\tau)}{\partial \tau}+\lambda\frac{\partial \overline{C}(\xi_i,\tau+\Delta\tau)}{\partial \tau}=\frac{\overline{C}(\xi_i,\tau+\Delta\tau)-\overline{C}(\xi_i,\tau)}{\Delta\tau}, \tag{5.14}$$

where λ is a weighted coefficient ($0\le\lambda\le1$).

Substituting equations (5.10) and (5.13) into equation (5.14) and considering the auxiliary condition (3.10), the drug release governing equation with time iteration is finally discretized in both spatial and time domains and reduced to a set of discrete algebraic equations in the following matrix form,

$$\begin{aligned}&\begin{bmatrix}[G_{ij}^{11}]_{N_T\times N_T} & [G_{ij}^{12}]_{N_T\times N_S}\\ [G_{ij}^{21}]_{N_S\times N_T} & [G_{ij}^{22}]_{N_S\times N_S}\end{bmatrix}\begin{Bmatrix}\{\overline{C}_i(\tau+\Delta\tau)\}_{N_T\times1}\\ \{\overline{C}_{\xi i}(\tau+\Delta\tau)\}_{N_S\times1}\end{Bmatrix} \\ &=\begin{bmatrix}[G_{ij}^{*11}]_{N_T\times N_T} & [G_{ij}^{*12}]_{N_T\times N_S}\\ [G_{ij}^{*21}]_{N_S\times N_T} & [G_{ij}^{*22}]_{N_S\times N_S}\end{bmatrix}\begin{Bmatrix}\{\overline{C}_i(\tau)\}_{N_T\times1}\\ \{\overline{C}_{\xi i}(\tau)\}_{N_S\times1}\end{Bmatrix},\end{aligned} \tag{5.15}$$

where

$$[G_{ij}^{11}]=[(1+\lambda\beta\Delta\tau)N_j(\xi_i)-\lambda\Delta\tau N_{j,\xi\xi}(\xi_i)], \tag{5.16-a}$$

$$[G_{ij}^{12}]=[-\frac{2\lambda\Delta\tau}{\xi_i}+(1+\lambda\beta\Delta\tau)(\xi_i-\sum_{n=1}^{N_T}N_n(\xi_i)\xi_n)]M_j(\xi_i), \tag{5.16-b}$$

$$[G_{ij}^{21}]=[G_{ij}^{*21}]=[N_{j,\xi}(\xi_i)], \tag{5.16-c}$$

$$[G_{ij}^{22}] = [G_{ij}^{*22}] = [(-\sum_{n=1}^{N_T} N_{n,\xi}(\xi_i)\xi_n)M_j(\xi_i)], \tag{5.16-d}$$

$$[G_{ij}^{*11}] = [(1-\lambda)\Delta\tau N_{j,\xi\xi}(\xi_i) + (1-\beta(1-\lambda)\Delta\tau)N_j(\xi_i)], \tag{5.16-e}$$

$$[G_{ij}^{*12}] = [(\frac{2(1-\lambda)\Delta\tau}{\xi_i} + (1-\beta(1-\lambda)\Delta\tau)(\xi_i - \sum_{n=1}^{N_S} N_n(\xi_i)\xi_n))M_j(\xi_i)]. \tag{5.16-f}$$

5.3 Numerical simulations and discussions

The experimentally measured nifedipine release data for the spherical nifedipine-loaded chitosan microgels exposed to phosphate buffer (pH 7.4), achieved by Filipovic et al. (1996) through the chitosan microgel preparation and characterization and nifedipine release determination, are simulated numerically by the present mathematical model. A series of B samples (B1~B5) are selected and the corresponding microgel radii R are listed in Table 5.1 (Filipovic et al., 1996). The totally loaded drug mass M_∞ listed in Table 5.1 are calculated based on the mass of drug-loaded microgels m(g), total drug content d(%), the mean radius of dry microgels R(cm) and the volume of the dissolution medium V(cm^3) obtained from the experimental data. Assuming that all drug is released and dissolved in the dissolution medium, $M_\infty = (4\pi R^3/3)\times(md/V)$. It is reminded that such an assumption will bring about unpredictable error in M_∞. However, since the ratio, M_t/M_∞, is concerned here, this inaccuracy would not affect the prediction.

5.3.1 Identification of physical parameters

Figure 5.1 shows the kinetics of *in vitro* drug release from the microgels with different microsphere radii and total initially loaded drug amounts. As the time

increases, the initial drug release amount increases rapidly, followed by a gradual drug release. B5 has larger microspheric radius R and higher total loaded drug amount M_∞ (see Table 5.1). It is observed that nifedipine from B5 is released a little faster than that from B1. Good agreement between numerically fitted results and experimental data is obtained for both B1 and B5 with the present mathematical model. It is seen that the model successfully captures the effect of micro spherical radius R. The values of the diffusion coefficient D, drug dissolution rate constant k and equivalent drug saturation concentration εC_s are identified by best-fitting the computed results to the experimental data. The identified D, k and εC_s are summarized in Table 5.1. The D value is found to be smaller than the reported value of nifedipine in cross-linked hydrogels of polyacrylamide-grafted guar gum (Soppimath et al., 2001). Generally the D values for various drugs in polymeric hydrogels range from 10^{-6} to 10^{-9} (cm^2/s). Several factors may contribute to the extremely low D value of nifedipine in the studied microgels. First, the solubility of nifedipine in the release medium is very low about 11 (μg/ml), which implies relatively large partition coefficient of nifedipine between the polymeric hydrogels and the release medium. Second, the microgels that are loaded with a high content of drug tend to absorb less water than those containing a lower content of drug so that the diffusion processed are retarded. Last, it is reported that an increase in drug content will also increase the crystallinity of the drug and thus slow down the release of such a crystalline drug (Soppimath et al., 2000).

Figure 5.2 illustrates the kinetics of nifedipine release from chitosan microgels with different network mesh parameters ε. These microgels are formed with the same nifedipine amount but different glutaraldehyde reaction times. With an increase in the

glutaraldehyde reaction time, the cross-linking degree of the microgels increases, which brings about a decrease in the network mesh parameter ε of the microgels. This results in the decrease of the equivalent saturation concentration εC_s. The fitting well represents the experimental results. The corresponding D and εC_s are identified by best-fitting the calculating results to the experimental data, and they are summarized in Table 5.1. The diffusion coefficient D is observed to be dependent on the cross-linking density, and thus on the network mesh parameter ε. The increase of εC_s from 0.823 to 1.225 increases the D value from 0.30×10^{-11} to 0.40×10^{-11} (cm^2/s). The increased network mesh parameter ε increases the drug diffusion coefficient D, which is in consistence with the findings by Pillay and Fassihi (1999).

Figures 5.1 and 5.2 validate that the present mathematical model is able to describe well the nifedipine release from chitosan microgels with different micro sphere conditions. It successfully captures the characteristics of the various important physical parameters affecting the kinetics of nifedipine release. Therefore, it is concluded that this model provides a suitable simulating approach to obtain deeper insight into the effects of the important physical parameters on drug release from the microgels.

5.3.2 Effect of physical parameters on drug release

In order to study the effect of the physical parameters on the kinetics of drug release, including the micro sphere radius R, drug diffusion coefficient D, drug dissolution rate constant k, and equivalent saturation concentration εC_s, the mathematical model is employed to simulate drug release kinetics. When the sensitivity study on one of the parameters is carried out, other parameters are

remained the same. In Figures 5.3 to 5.6, the experimental data of drug release from B5 sample are taken as a comparative example.

Figure 5.3 shows the effect of micro spherical mean radius R on the controlled drug release, where the drug diffusion coefficient $D=0.4\times10^{-11}$(cm^2/s), drug dissolution rate constant $k=7.0\times10^{-7}$ (s^{-1}), and drug equivalent saturation concentration $\varepsilon C_s=1.225\times10^{-6}$ (g/cm^3). The micro sphere radius R in the figure ranges from 9.5×10^{-4} to 17.0×10^{-4} (cm). With increasing the micro sphere radius R, the overall drug release rate becomes slower. It is noted that a slight change of micro sphere radius R results in remarkable alteration of nifedipine release rate. A smaller microgel has larger specific surface area of contact with the release medium, and facilitate the drug diffusion through the continuous matrices of microgels into the release medium in comparison with a larger microgel. A decrease in micro sphere radius R increases both the initial fast release rate and the following gradual release rate. This implicates that variation of micro spheric radius R affects both drug dissolution and diffusion process.

The effect of equivalent drug saturation concentration εC_s on drug release kinetics is shown in Figure 5.4, where the equivalent drug saturation concentration εC_s changes from 0.5×10^{-6} to 1.7×10^{-6} (g/cm^3). The drug release remarkably increases with increasing porosity. An increase of the network mesh parameter ε of microgels, i.e. a decrease of the cross-linking density of microgels, simultaneously increases the drug equivalent saturation concentration εC_s and the drug diffusion coefficient D, which results in an increase in both drug dissolution and diffusion rates. These synergically lead to the increased nifedipine release rate.

Figure 5.5 is obtained for discussion about the effect of drug diffusion coefficient D on the drug release, where the value of D varies from 0.012×10^{-11} to 4.0×10^{-11} (cm^2/s). It is observed that the diffusion process controls significantly the initial drug release stage. As the diffusion coefficient D increases, the initial drug release rate increases distinctly, and the drug release amount becomes a linear function of time at relatively shorter times. However, after a certain period of release time, the drug release arrives at a constant level. This indicates that the release of drug with lower diffusion coefficient D is via diffusion mechanism, whereas the diffusion process does not solely control the release of drug with higher diffusion coefficient D.

Figure 5.6 illustrates the effect of the drug dissolution rate constant k on drug release, where the dissolution rate constant k varies from 0.70×10^{-7} to 24.0×10^{-7} (s^{-1}) It is manifest that alteration of drug dissolution rate constant k has insignificant effects on initial drug release rate. However, after a period of release time, the drug release rate increases with increasing dissolution rate constant k. This indicates that different mechanisms control different drug release stages. At the initial stage, diffusion through continuous matrices of microgels predominantly affects the drug release. After a period of drug release, drug dissolution starts to significantly affect the drug release rate.

5.4 A brief remark

The present mathematical model based on both drug dissolution and diffusion through the continuous matrices of microgels is well validated by comparison with the experimental nifedipine release from the spherical chitosan microgels. It provides a better understanding of the underlying mechanisms in micro spheric drug release system, and represents a highly efficient tool to study the roles played by important

parameters of the drug and the microgels such as the diffusion coefficient, the micro spherical radius and the network mesh parameter. Consequently, it can be used to analyze and optimize the design of the controlled drug release process.

Table 5.1 Experimental and identified parameters of nifedipine microgels.

Type	Experimental data (Filipovic et al., 1996)		Identified parameters		
	R ($\times 10^{-4}$cm)	M_∞ ($\times 10^{-13}$g)	D ($\times 10^{-11}$cm^2/s)	k ($\times 10^{-7}$s^{-1})	εC_s ($\times 10^{-6}$ g/cm^3)
B1	12.10	0.20	0.40	7.0	1.225
B2	13.90	0.24	0.40	7.0	1.225
B3	13.05	0.20	0.35	7.0	1.033
B4	12.20	0.16	0.30	7.0	0.823
B5	14.50	0.32	0.40	7.0	1.225

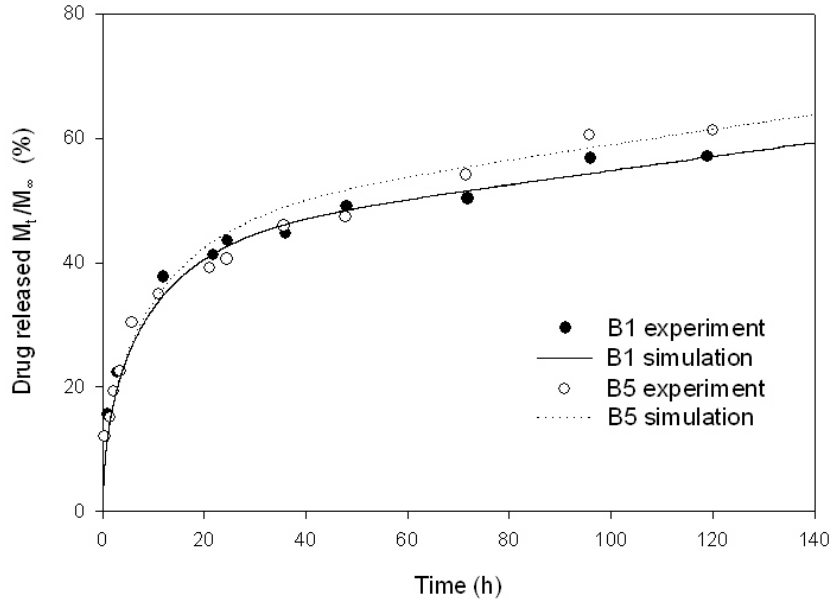

Figure 5.1 Rate of nifedipine release from chitosan microgels with different radii *R*.

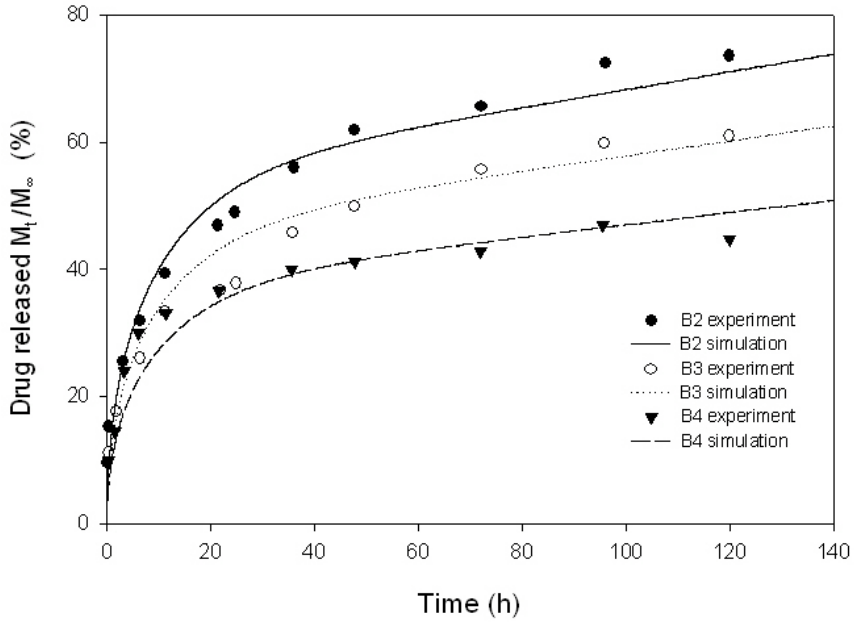

Figure 5.2 Rate of nifedipine release from chitosan microgels with different network mesh parameter ε.

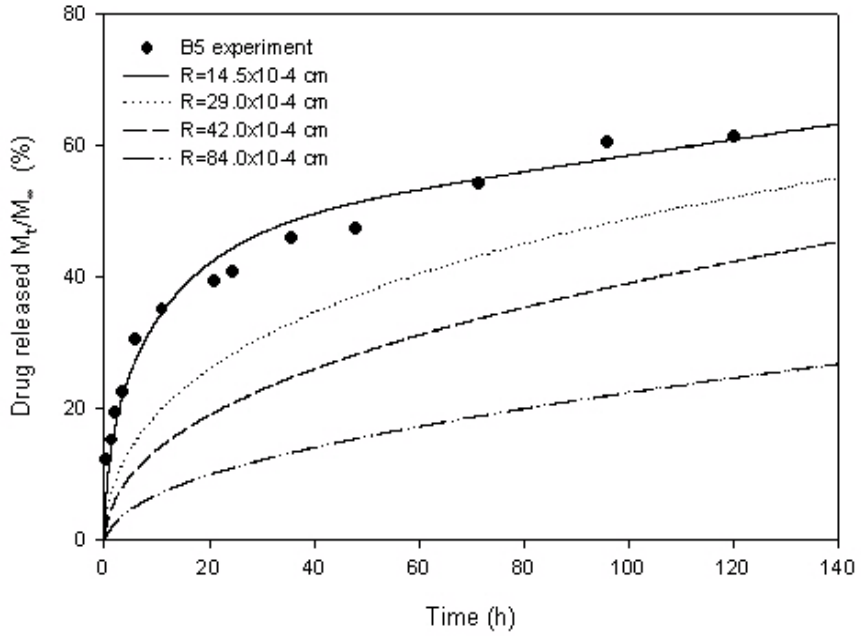

Figure 5.3 Effect of the microsphere radius R on the rate of nifedipine release from chitosan microgels when D=0.4×10^{-11} cm^2/s, k=7.0×10^{-7} s^{-1}, εC_s =1.225×10^{-6} g/cm3.

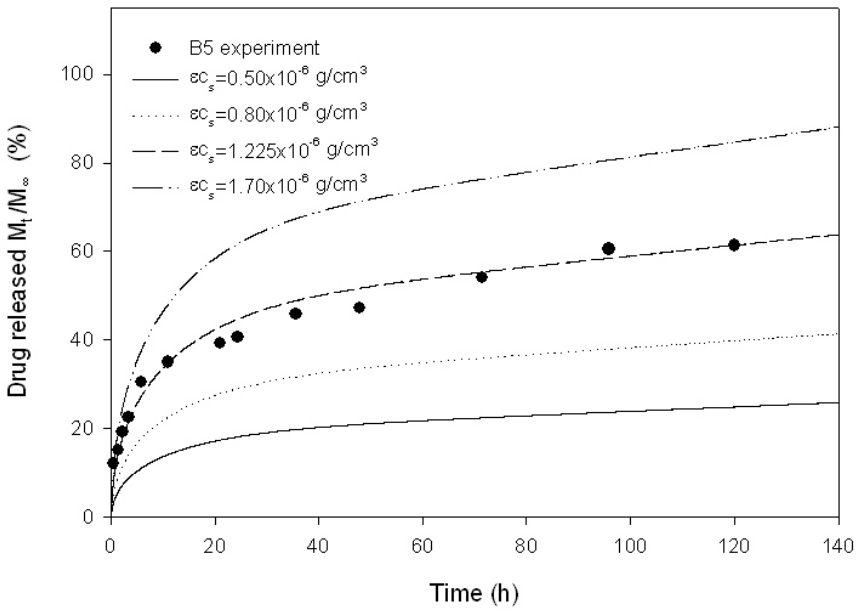

Figure 5.4 Effect of the equivalent drug saturation concentration εC_s on the rate of nifedipine release from chitosan microgels when D=0.4×10^{-11} cm^2/s, R=14.5×10^{-4} cm, k=7.0×10^{-7} s^{-1}.

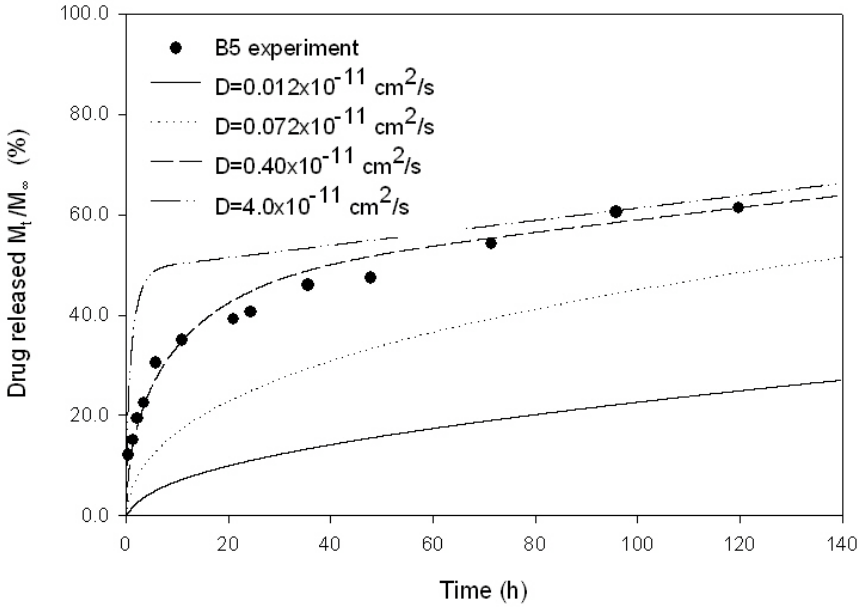

Figure 5.5 Effect of the diffusion coefficient D on the rate of nifedipine release from chitosan microgels when R=14.5×10^{-4} cm, k=7.0×10^{-7} s^{-1}, εC_s=1.225×10^{-6} g/cm^3.

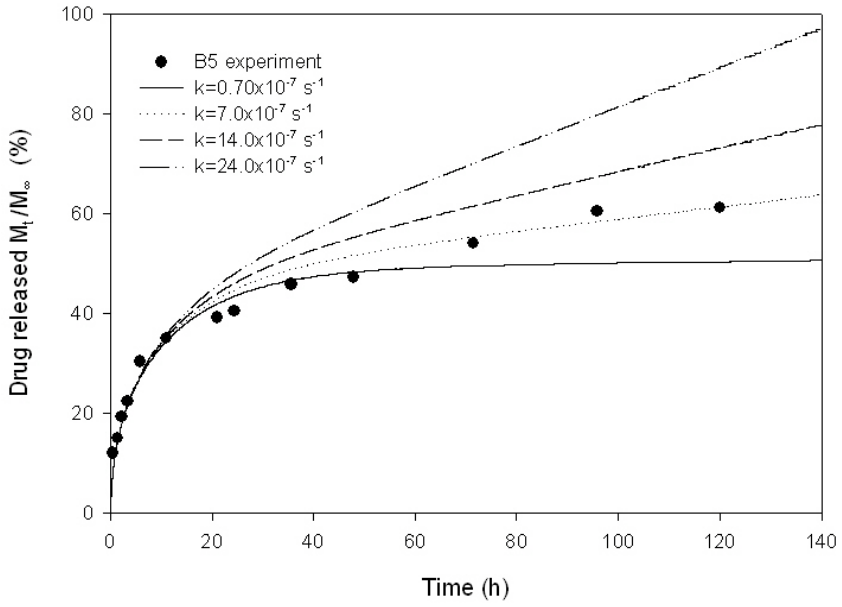

Figure 5.6 Effect of the dissolution rate constant k on the rate of nifedipine release from chitosan microgels for R=14.5×10^{-4} cm, D=0.4×10-11 cm^2/s, εC_s=1.225×10^{-6} g/cm^3.

Chapter 6

Conclusions and Future Works

A summation of the conclusions based on the present studies and discussions is presented in this chapter. This is followed by a brief presentation of recommendable studies for future works.

6.1 Conclusions

In this dissertation, two mathematical models are presented for simulation of hydrogel behaviors. One is the steady-state MECtherm model to simulate the swelling equilibrium of thermo-sensitive hydrogels, and the other is the transient model to investigate the drug delivery from microgels.

In the study of swelling equilibrium of thermo-sensitive hydrogels, a novel multiphysical steady-state model, termed the Multi-Effect-Coupling thermal-stimulus (MECtherm) model, has been developed to simulate and predict the swelling equilibrium for neutral and ionized thermo-sensitive hydrogels with the volume phase transition. The developed mathematical model consists of the steady-state Nernst-Planck equations, Poisson equation and swelling equilibrium governing equation. In order to solve the multi-field coupling system with both nonlinear partial differential equations and transcendental equation, a hierarchical Newton iteration strategy is implemented in the computational flow chart, and the meshless Hermite-cloud method is employed for numerical simulation of the responsive hydrogels subject to an environmental temperature change. The simulated relations between temperature and volume swelling ratio are in good agreement with experimental data. In parameter

studies, the influence of various physical parameters, including the initial fixed charge density, electrolyte solution concentration, crosslink density and initial volume fraction, on the responsive behaviors of the thermal-sensitive hydrogels are investigated in details. Distributions of mobile ion concentrations, fixed charge densities as well as the electric potentials in both interior hydrogels and exterior bathing solution are also simulated and discussed. It should be noted that the degree of swelling can be improved by increasing the initial fixed charge density, or by decreasing the electrolyte solution concentration. The present studies and discussions provide useful information for the BioMEMS designers to enhance the performance of the responsive hydrogels in BioMEMS as critically active sensing/actuating elements, such as micro actuators, micro valves, chemical sensors and other components.

In the study of microgel-based drug delivery system, the controlled nifedipine release from chitosan spherical microgels is simulated numerically with a mathematical model. The numerically simulating investigations provide deeper insight into the drug release mechanisms, and elucidate efficiently the influences of various physical parameters. The present mathematical model takes into account both drug dissolution and diffusion through the continuous matrices of the spherical microgels. Meshless Hermite-cloud method is also employed to solve the formulated governing partial differential equations. It is seen that the model describes well the kinetics of nifedipine release process from the spherical chitosan microgels. The numerical investigation provides a better understanding of the underlying mechanisms in microspheric drug release system and a high-efficient tool to study the roles played by important characteristics of the drug and the microgels. The effects of several physical parameters, such as microsphere radius, equivalent drug saturation

concentration, drug diffusion coefficient, and drug dissolution rate constant on drug release are evaluated in details. They are useful for practical designers to analyze and optimize the controlled drug release process.

6.2 Suggestion for future works

Currently, the present work focuses on the temperature sensitive hydrogels. It is highly desirable to make further investigations of phase transitions incorporating with other environmental stimuli, such as pH, electric field, glucose and so on. The studies on these coupling stimuli may lead to possibilities to create new kinds of responsive hydrogels.

In the present work, the model simulating the drug delivery from microgels assumes that the drug diffusivity in the membrane remains constant during transportation. A recommended study is development of mathematical models with incorporation of time-dependent diffusivities that reflect the effect of drug concentration on the drug transportation rate through membrane.

References

Aluru, N.R. A point collocation method based on reproducing kernel approximations, International Journal for Numerical Methods in Engineering, 47, pp.1083-1121. 2000.

Aluru, N.R. and G. Li. Finite cloud method: a true meshless technique based on a fixed reproducing kernel approximation, International Journal for Numerical Methods in Engineering, 50, pp.2373-2410. 2001.

Annaka, M., Motokawa, K., Sasaki, S., Nakahira, T., Kawasaki, H., Maeda, H., Amo, Y. and Y. Tominaga. Salt-induced volume phase transition of poly(N-isopropylacrylamide) gel, Journal of Chemical Physics, *113*, pp.5980-5985. 2000.

Atluri, S.N., Cho, J.Y. and H.G. Kim. Analysis of thin beams, using the meshless local Petrov-Galerkin (MLPG) method, with generalized moving least squares interpolation, Computational Mechanics, *24*, pp.334-347. 1999a.

Atluri, S.N., Cho, J.Y. and H.G. Kim. A critical assessment of the truly meshless local Petrov-Galerkin (MLPG), and local boundary integral Equation (LBIE) methods, with generalized moving least squares interpolation, Computational Mechanics, *24*, pp.348-372. 1999b.

Atluri, S.N. and S.P. Shen. The meshless local Petrov-Galerkin (MLPG) method. Tech Science Press. Encino USA. 2002.

Atluri, S.N. and T. Zhu. A new meshless local Petrov-Galerkin (MLPG) approach in computational mechanics, Computational Mechanics, *22*, pp.117-127. 1998.

Atluri, S.N. and T. Zhu. The meshless local Petrov-Galerkin (MLPG) approach for solving problems in elsto-statics, Computational Mechanics, *25*, pp.169-179. 2000.

Bae, Y.C., Shim, J.J., Soane, D.S. and J.M. Prausniz. Representation of vapor-liquid and liquid-liquid equilibria for binary systems containing polymers: Applicability of an extended Flory-Huggins equation, Journal Applied Polymer Science, *47*, pp.1193-1206. 1993.

Beltran, S., Hooper, H.H., Blanch, H.W. and J.M. Prausnitz. Swelling equilibria for ionized temperature-sensitive gels in water and in aqueous salt solutions, Journal of Chemical Physics, *92*, pp.2061-2066. 1990.

Belytschko, T., krongauz, Y., Organ, D., Fleming, M. and P. Krysl. Meshless method: an overview and recent development. Computer Methods in Applied Mechanics and Engineering, *139*, pp.3-47. 1996.

Belytschko, T., krysl, P. and Y. Krongauz. A three-dimensional explicit element-free Galerkin method, International Journal for Numerical Methods in Fluids, *24*, pp.1253-1270. 1997.

Belytschko, T., Lu, Y.Y. and L. Gu. Element free Galerkin methods, International Journal for Numerical Methods in Engineering, *37*, pp.229-256. 1994.

Belytschko, T., Lu, Y.Y. and L. Gu. Element free Galerkin methods for static and dynamic fracture, International Journal of Solids and structures, *32*, pp.2547-2570. 1995.

Birshtein, T.M. and V.A. Pryamitsyn. Coil-globule type transitions in polymers. 2. Theory of coil-globule transition in linear macromolecules, Macromolecules, *24*, pp.1554-1560. 1991.

Benz, W. Smooth particle hydrodynamics: a review. In: Numerical Modeling of Non-linear Stellar Pulsation: Problems and Prospects. Kluwer Academic, Boston. 1990.

Chandy, T. and C.P. Sharma. Chitosan beads and granules for oral sustained delivery of nifedipine: in vitro studies, Biomaterials, *13*, pp949-952. 1992.

Crank, J. The Mathematics of Diffusion. 2nd Edition, Oxford: Clarendon Press. 1975.

Cussler, E.L., Stokar, M.R. and J.E. Varberg. Gels as size selective extraction solvents, American Institute of Chemical Engineers Journal, *30*, pp.578–582. 1984.

Dhawan, S. and A.k. Singla. Nifedipine loaded chitosan microspheres prepared by emulsification phase-separation, Biotechnic and Histochemistry, *78*, pp.243 - 254. 2003.

Duarte, C.A. and J.T. Oden. An h-p adaptive method using clouds, Computer Methods in Applied Mechanics and Engineering, *139*, pp.237-262. 1996.

Dusek, K. and D. Patterson. Transition in swollen polymer networks induced by intramolecular condensation, Journal of Polymer Science: Polymer Physics, *6*, pp.1209-1216. 1968.

Erman, B. and P.J. Flory. Critical phenomena and transitions in swollen polymer networks and in linear macromolecules, Macromolecules, *19*, pp.2342-2353. 1986.

Franke, C. and R. Schaback. Solving partial differential equations by collocation using radial basis functions, Applied Mathematics and Computation, *93*, pp.73-82. 1997.

Filipovic-Grcic, J., Becirevic-Lacan, M., Skalko, N. and I. Jalsenjak. Chitosan microspheres of nifedipine and nifedipine-cyclodextrin inclusion complexes, International Journal of Pharmaceutics, *135*, pp.183-190. 1996.

Flory, P. J. Principles of polymer chemistry. Cornell University Press. 1953.

Gehrke, S.H. Synthesis, Equilibrium swelling, kinetics, permeability and applications of environmentally responsive gels, Responsive Gels: Volume Transitions II. pp.81-144, Springer-Verlag Berlin Heidelberg Press. 1993.

Gehrke, S.H. and E.L. Cussler. Mass transfer in pH-sensitive hydrogels, Chemical Engineering Science, *44*, pp.559-566. 1989.

Gingold, R.A. and J.J. Monaghan. Smooth particle hydrodynamics: theory and applications to non-spherical stars, Monthly Notices of the Royal Astronomical Society, *181*, pp.375-389. 1977.

Grassi, M., Colombo, I. and R. Lapasin. Drug release from an ensemble of swellable crosslinked polymer particles, Journal of Controlled Release, *68*, pp.97-113. 2000.

Grimshaw, P.E., Nussbaum, J.H., Grodzinsky, A.J. and M.L. Yarmush. Kinetics of electrically and chemically induced swelling in polyelectrolyte gels, Journal of Chemical Physics, *93*, pp.4462-4468. 1990.

Grossman, E., Messerli, F.H., Grodzicki, T. and P. Kowey. Should a moratorium be placed on sublingual nifedipine capsules given for hypertensive emergencies and pseudoemergencies, Journal of the American Medical Association, *276*, pp.1328-1331. 1996.

Gu, Y.T. and G.R. Liu. A meshless local Petrov-Galerkin (MLPG) method for free and forced vibration analyses for solids, Computational mechanics, *27*, pp.188-198. 2001a.

Gu, Y.T. and G.R. Liu. A meshless local Petrov-Galerkin (MLPG) formulation for static and free vibration analyses of thin plates, Computer Modeling in Engineering & Sciences, *2*, pp.463-476. 2001b.

Gu, Y.T. and G.R. Liu. A local point interpolation method for static and dynamic analyses of thin beams, Computer Methods in Applied Mechanics and Engineering, *190*, pp.5515-5528. 2001c.

Gu, Y.T. and G.R. Liu. A coupled element free Galerkin/Boundary element method for stress analysis of two-dimensional solids, Computer Methods in Applied Mechanics and Engineering, *190*, pp.4405-4419. 2001d.

Gu, Y.T. and G.R. Liu. A boundary point interpolation method for stress analyses of solids, Computational Mechanics, *28*, pp.47-54. 2002.

Gu, Y.T. and G.R. Liu. A boundary radial point interpolation method (BRPIM) for 2-D structural analyses, Structural Engineering and Mechanics, An International Journal. *15*, pp.535-550. 2003a.

Gu, Y.T. and G.R. Liu. Hybrid boundary point interpolation methods and their coupling with the element free Galerkin method, Engineering Analysis with Boundary Elements, *27*, pp.905-917. 2003b.

Harland, R.S., Dubernet, C., Benoit, J.P. and N.A. Peppas. A model of dissolution-controlled, diffusional drug release from non-swellable polymeric microspheres, Journal of Controlled Release, *7*, pp.207-215. 1988.

Hegen, D. Element-free Galerkin methods in combination with finite element approaches, Computer Methods in Applied Mechanics and Engineering, *135*, pp.143-166. 1996.

Higuchi, T. Rate of release of medicaments from ointment bases containing drugs in suspension, Journal of Pharmaceutical Sciences, *50*, pp.874-878. 1961.

Higuchi, W.I. Analysis of data on the medicament release from ointments, Journal of Pharmaceutical Sciences, *51*, pp.802-805. 1962.

Hino, T. and J.M. Prausnitz. Molecular thermodynamics for volume-change transitions in temperature-sensitive polymer gels, Polymer, 39, pp.3279-3283. 1998.

Hirokawa, Y. and Tanaka, T. Volume phase transition in a nonionic gel, Journal of Chemical Physics, *81*, pp.6379-6380. 1984.

Hirotsu, S., Hirokawa, Y. and T. Tanaka. Volume-phase transitions of ionized N-isopropylacrylamide gels, Journal of Chemical Physics, *87*, pp.1392-1395. 1987.

Hirotsu, S. Softenning of bulk modulus and negative Poisson's ratio near the volume phase transition of polymer gels, Journal of Chemical Physics, *94*, pp.3949-3957. 1991.

Hoffman, A.S. Applications of thermally reversible polymers and hydrogels in therapeutics and diagnostics, Journal of Controlled Release, *6*, pp.297-305. 1987.

Hombreiro-Perez, M., Siepmann, J., Zinutti, C., Lamprecht, A., Ubrich, N., Hoffman, M., Bodmeier, R. and P. Maincent. Non-degradable microparticles containing a hydrophilic and/or a lipophilic drug: preparation, characterization and drug release modeling, Journal of Controlled Release, *88*, pp.413-428. 2003.

Hong, Y.P. and Y.C. Bae. Phase behaviors of partially ionized hydrogels in aqueous salt solutions: Applicability of the modified double-lattice model, Journal of Polymer Science: Polymer Physics, *40*, pp.2333-2338. 2002.

Hooper, H.H., Baker, J.P., Blanch, H.W. and J.M. Prausinitz. Swelling equilibria for positively ionized polyacrylamide hydrogels, Macromolecules, *23*, pp.1096-1104. 1990.

Ilavsky, M., Hrouz, J. and K. Ulbrich. Phase transition in swollen gels. 3. The temperature collapse and mechanical behavior of poly(N,N-diethylacrylamide) networks in water, Polymer Bulletin, *7(2-3)*, pp.107-113. 1982.

Katayama, S., Hirokawa, Y. and T. Tanaka. Reentrant phase transition in acrylamide-derivative copolymer gels, Macromolecules, *17*, pp.2641-2643. 1984.

Kato, E. Pressure-induced volume phase transition of polyacrylamide gels in acetone–water mixtures, Journal of Chemical Physics, *113*, pp.1310-1314. 2000.

Katchalsky, A. Rapid swelling and deswelling of reversible gels of polymeric acids by ionization, Experientia**,** *5*, pp.319-320. 1949.

Lele, A.K., Badiger, M.V., Hirve, M.M. and R.A. Mashelkar. Thermodynamics of hydrogen-bonded polymer gel-solvent systems, Chemical Engineering Science, *50*, pp.3535-3542. 1995.

Lele, A.K., Karode S.K., Badiger M.V. and R.A. Mashelkar. Prediction of re-entrant swelling behavior of poly(N-isopropyl acrylamide) gel in a mixture of ethanol–water using lattice fluid hydrogen bond theory, Journal of Chemical Physics, *107*, pp.2142-2148. 1997.

Li, H., Ng, T.Y., Cheng, J.Q. and K.Y. Lam. Hermite-Cloud: a novel true meshless method, Computational Mechanics, *33*, pp.30-41. 2003.

Li, Y. and T. Tanaka. Phase Transitions of Gels, Annual Review of Material Science, *22*, pp.243-276. 1992.

Li, S.F. and W.K. Liu. Meshfree and particle methods and their application, Applied Mechanics Reviews, *55*, pp.1-34. 2002.

Liu, G.R., Dai, K.Y., Lim, K.M. and Y.T. Gu. A Radial Point Interpolation Method for Simulation of Two-dimensional Piezoelectric Structures, Smart Materials and Structures, *12*, pp.171-180, 2003.

Liu, G.R. Mesh Free Methods: Moving Beyond the Finite Element Method. New York: Chemical Rubber Company Press. 2002.

Liu, G.R. and Y.T. Gu. Meshless local Petrov-Galerkin (MLPG) method in combination with finite element and boundary element approaches, Computational Mechanics, *26*, pp.536-546, 2000a.

Liu, G.R. and Y.T. Gu. Coupling of element free Galerkin and hybrid boundary element methods using modified variational formulation, Computational Mechanics, *26*, pp.166-173, 2000b.

Liu, G.R. and Y.T. Gu. A point interpolation method for two dimensional solids, International Journal of Numerical Methods in Engineering, *50*, pp.937-951, 2001a.

Liu, G.R. and Y.T. Gu. A local radial interpolation method for stress analysis of two-dimensional solids, Structural Engineering and Mechanics, *11*, pp.221-236. 2001b.

Liu, G.R. and Y.T. Gu. A local radial interpolation method (LRPIM) for free vibration analysis of 2-D solids, Journal of Sound Vibration, *246*, pp.29-46. 2001c.

Liu, G.R., Gu, Y.T. and K.Y. Dai. Assessment and applications of point interpolation methods for computational mechanics, International Journal of Numerical Methods in Engineering, *59*, pp.1373-1397. 2004.

Liu, G.R. and Y.T. Gu. Comparisons of two meshfree local point interpolation methods for structural analysis, Computational Mechanics, *29*, pp.107–121, 2002.

Liu, G.R. and Y.T. Gu. An introduction to meshfree methods and their programming. Kluwer Academic Publishers (in press).

Liu, W.K., Han, W.M., Lu, H.S., Li, S.F. and J. Cao. Reproducing kernel element method, Part I: Theoretical formulation, Computer Methods in Applied Mechanics and Engineering, *193*, pp.933-951. 2004.

Liu, W.K., Li, S. and T. Belytschko. Moving least square reproducing kernel method Part I: Methodology and convergence, Computer Methods in Applied Mechanics and Engineering, *143*, pp.422-453. 1997.

Liu, W.K., Chen, Y., Chang, C.T. and T. Belytschko. Advances in multiple scale kernel particle methods, Computational Mechanics, *18*, pp.73-111. 1996a.

Liu, W.K., Chen, Y., Chang, J.S., Belytschko, T., Uras, R.A. and C.T. Chang. Overview and applications of the reproducing kernel particle methods, Archives in Computational Methods in Engineering State of the Art Review, *3*, pp.3-80. 1996b.

Liu, W.K., Chen, Y.J., Uras, R.A. and C.T. Chang. Generalized multiple scale reproducing kernel particle methods, Computer Methods in Applied Mechanics and Engineering, *139*, pp.91-158. 1996c.

Liu, W.K., Jun, S. and Y.F. Zhang. Reproducing kernel particle methods, International Journal for Numerical Methods in Fluids, *20*, pp.1081-1106. 1995.

Liu, X., Liu, G.R., Tai, K. and K.Y. Lam. Radial basis point interpolation collocation method for 2-D solid problem, In: Advances in Meshfree and X-FEM methods, Proceedings of the 1st Asian Workshop on Meshfree Methods, Liu, G. R. (ed.), World Scientific, pp.35-40. 2002.

Liu, L.X., Ku, J., Khang, G., Lee, B., Rhee, J.M. and H.B. Lee. Nifedipine controlled delivery by sandwiched osmotic tablet system, Journal of Controlled Release, *68*, pp.145-156. 2000.

Liszka, T. An interpolation method for an irregular net of nodes, International Journal for Numerical Methods in Engineering, *20*, pp.1599-1612. 1984.

Liszka, T.J., Duarte, CAM. and W.W. Tworzydlo. hp-meshless cloud method, Computer Methods in Applied Mechanics and Engineering, *139*, pp.263-288. 1996.

Lu, Y.Y., Belytschko, T. and L. Gu. A new implementation of the element free Galerkin method, Computer Methods in Applied Mechanics and Engineering, *113*, pp.397-414. 1994.

Mamada, A., Tanaka, T., Kungwatchakun, D. and M. Irie. Photo induced phase transition of gels, Macromolecules, *23*, pp.1517-1519. 1990.

Mansoor, A.F. and L.A. von Hagel Keefer. The dangers of immediate-release nifedipine for hypertensive crises, Pharmacy and Therapeutics, *27*, pp.362-365. 2002.

Marchetti, M., Prager, S. and E.L. Cussler. Thermodynamic predictions of volume changes in temperature-sensitive gels. 1. Theory, Macromolecules, *23*, pp.1760-1765. 1990,

Marchetti, M., Prager, S. and E.L. Cussler. Thermodynamic predictions of volume changes in temperature-sensitive gels. 2. Experiments, Macromolecules, *23*, pp.3445-3450. 1990.

Melenk, J.M. and I. Babuska. The partition of unity finite element method: basic theory and applications, Computer Methods in Applied Mechanics and Engineering, *139*, pp.289-314. 1996.

Monaghan, J.J. Particle methods for hydrodynamics, Computer Physics reports, *3*, pp.71-124. 1985.

Moerkerke, R., Koningsveld, R., Berghmans, H., Dusek, K. and K. Solc. Phase Transitions in Swollen Networks, Macromolecules, *28*, pp.1103-1107. 1995.

Mukherjee, Y.X. and S. Mukherjee. On boundary conditions in the element method: diffuse approximation and diffuse elements, Computational mechanics, *19*, pp.267-270. 1997.

Nayroles, B., Touzot, G. and P. Villon. Generalizing the finite element method: diffuse approximation and diffuse elements, Computational Mechanics, *10*, pp.307-318. 1992.

Ng, T.Y., Li, H., Cheng, J.Q. and K.Y. Lam. A new hybrid meshless-differential order reduction (hM-DOR) method with applications to shape control of smart structures via distributed sensors/actuators, Engineering Structures, *25*, pp.141-154. 2003.

Oflate, E., Idelsohn, S., Zienkiewicz, O.Z. and R.L. Taylor. A finite point method in computational mechanics. Applications to convective transport and fluid flow, International Journal of Numerical Methods in Engineering, *39*, pp.3839-3867. 1996.

Ohs, R.R. and N.R. Aluru. Meshless analysis of piezoelectric devices, Computational Mechanics, 27, pp23-36. 2001.

Ohmine, I. and T. Tanaka. Salt effects on the phase transition of ionic gels, Journal of Chemical Physics, *77*, pp.5725-5729. 1982.

Onate, E., Idelsohn, S., Zienkiewicz, O.C. and R.L. Taylor. A finite point method in computational mechanics. Applications to convective transport and fluid flow,

International Journal for Numerical Methods in Engineering, *39*, pp.3839-3866. 1996a.

Onate, E., Idelsohn, S., Zienkiewicz, O.C., Taylor, R.L. and C. Sacco. A stabilized finite point method for analysis of fluid mechanics problems, Computer Methods in Applied Mechanics and Engineering, *139*, pp.315-346. 1996b.

Onate, E. and S. Idelsohn. A mesh-free finite point method for advective-diffusive transport and fluid flow problems, Computational Mechanics, *21*, 283-292. 1998.

Onuki, A. Theory of Phase Transition in Polymer Gels, Responsive Gels: Volume Transitions I. pp.63-122, Springer-Verlag Berlin Heidelberg Press. 1993.

Otake, K., Inomata, H., Konno, M. and S. Saito. A new model for the thermally induced volume phase transition of gels, Journal of Chemical Physics, *91*, pp.1345-1350. 1989.

Otake, K., Inomata, H., Konno, M. and S. Saito. Thermal Analysis of Volume Phase Transition with N-Isopropylacrylamide Gels, Macromolecules, *23*, pp.283-289. 1990.

Painter, P.C., Graft, J. and M.M. Coleman. A lattice model describing hydrogen bonding in polymer mixtures, Journal of Chemical Physics, *92*, pp.6166-6174. 1990.

Perrone, N. and R. Kao. A general finite difference method for arbitrary meshless, Computers & Structures, *5*, pp.45-58. 1975.

Prange, M.M., Hooper, H.H. and J.M. Prausnitz. Thermodynamics of aqueous systems containing hydrophilic polymers or gels, American Institute of Chemical Engineers Journal, *35*, pp.803-813. 1989.

Pillay, V. and R. Fassihi. A New Method for Dissolution Studies of Lipid-Filled Capsules Employing Nifedipine as a Model Drug, Pharmaceutical Research, *16*, pp.333-338. 1999.

Roberto, F.S. Freitas and E.L. Cussler. Temperature sensitive gels as extraction solvents, Chemical Engineering Science, *44*, pp.97-103. 1987.

Roseman, T.J. and W.I. Higuchi. Release of medroxy progesterone acetate from a silicone polymer, Journal of Pharmaceutical Sciences, *59*, pp.353-358. 1970.

Samson, E., Marchand, J., Robert, J.L. and J.P. Bournazel. Modelling ion diffusion mechanisms in porous media, International Journal for Numerical Methods in Engineering, *46*, pp.2043-2060. 1999.

Sanchez, I.C. and R.H. Lacombe. An elementary molecular theory of classical fluids, Pure fluids, Journal of Physical Chemistry, *80*, pp.2352-2362. 1976.

Sanchez, I.C. and R.H. Lacombe. Statistical Thermodynamics of Polymer Solutions, Macromolecules, *11*, pp.1145-1156. 1978.

Sasaki, S. and H. Maeda. Simple theory for volume phase transition of hydrated gels, Physical Review E, *54*, pp.2761-2765. 1996.

Shibayama, M. and T. Tanaka. Volume Phase Transition and Related Phenomena of Polymer Gels, Responsive Gels: Volume Transitions II. pp.1-62, Springer-Verlag Berlin Heidelberg Press. 1993.

Shirota, H., Endo, N. and K. Horie. Volume phase transition of polymer gel in water and heavy water, Chemical Physics, *238*, pp.487-494. 1998.

Soppimath, K.S., Kulkarni, R.A. and T.M. Sminsbhavi. Controlled release of antihypertensive drug from the interpenetrating network poly(vinyl alcohol)-guar gum hydrogel microspheres, Journal of Biomaterials Science, Polymer Edition, *11*, pp.27-44. 2000.

Soppimath, K.S., Kulkarni, A.R. and T.M. Aminabhavi. Chemically modified polyacrylamide-g-guar gum-based crosslinked anionic microgels as pH-sensitive drug delivery systems: preparation and characterization, Journal of Controlled Release, *75*, pp.331-345. 2001.

Soppimath, K.S. and T.M. Aminabhavi. Ethyl acetate as a dispersing solvent in the production of poly(DL-lactide-co-glycolide) microspheres: effect of process parameters and polymer type, Journal of Microencapsulation, *19*, pp.281-292. 2002.

Tanaka, T. Collapse of Gels and the Critical Endpoint, Physical Review Letters, *40*, pp.820–823. 1978.

Tanaka, T., Fillmore, D., Sun, S.T., Nishio, I., Swislow, G. and A. Shah. Phase Transitions in Ionic Gels, Physical Review Letters, *45*, pp.1636-1639. 1980.

Tanaka, T. Gels, Scientific American, *244*, pp.110-124. 1981.

Tang, Z., Shen, S. and S.N. Atluri1. Analysis of Materials with Strain-Gradient Effects: A Meshless Local Petrov-Galerkin(MLPG) Approach, with Nodal Displacements only, Computer Modelling in Engineering & Sciences, *4*, pp.177-196. 2003.

Varghese, S., Lele, A.K. and R.A. Mashelkar. Designing new thermo reversible gels by molecular tailoring of hydrophilic-hydrophobic interactions, Journal of Chemical Physics, *112*, pp.3063-3070. 2000.

Varshosaz, J. and M. Falamarzian. European Drug diffusion mechanism through pH-sensitive hydrophobic/polyelectrolyte hydrogel membranes, Journal of Pharmaceutics and Biopharmaceutics, *51*, pp.235-240. 2001.

Wang, K.L., Burban J.H. and E.L. Cussler. Hydrogels as Separation Agents, Responsive Gels: Volume Transitions II. pp.67-80, Springer-Verlag Berlin Heidelberg Press. 1993.

Wolf, B.A. Thermodynamic theory of flowing polymer solutions and its application to phase separation, Macromolecules, *17*, pp.615-618. 1984.

Zhang, X., Liu, X.H., Song, K.Z. and M.W. Lu. Least-squares collocation meshless method, International Journal of Numerical Methods in Engineering, *51*, pp.1089-1100. 2001.

Zoller, P. Analysis of the equation of state of polymer melts in terms of the Ising fluid model, Journal of Polymer Science: Polymer Physics, *18*, pp.157-160. 1980.

Zoller, P. Evaluation of the PVT relationships of seven polymer melts in terms of the equation of state of Flory, Orwoll, and Vrij, Journal of Polymer Science: Polymer Physics, *18*, pp.897-901. 1980.

Publications Arising from Thesis

1. H. Li, G.P. Yan, S.N. Wu, Z.J. Wang and K.Y. Lam, Numerical simulation of controlled nifedipine release from chitosan microgels, Journal of Applied Polymer Science (in press).

2. X.G. Wang, H. Li and Z.J. Wang, Multiphysic-field model development and simulation for volume phase transition of ionic thermosensitive hydrogels, International Conference on Scientific and Engineering Computation, 30 June ~ 2 July 2004, Singapore (assigned number 0165).

3. X.G. Wang, H. Li, Z.J. Wang and K.Y. Lam, Multiphysically modeling and meshless simulation of ionized thermo-sensitive hydrogels in swelling equilibrium, Journal of Controlled Release (submitted).